





ORIGINAL ARTICLE

Exploring copyrolysis characteristics and thermokinetics of peach stone and bituminous coal blends

Asif Hussain Khoja¹  | Hamad Gohar¹ | Waqar Ul Habib Khan¹ |
 Umair Yaqub Qazi² | Israf Ud Din³ | Abdulaziz Al-Anazi⁴ |
 Waqar Muhammad Ashraf⁵  | M. A. Mujtaba⁶  | Fahid Riaz⁷  |
 Syed Sheraz Daood⁸

¹Fossil Fuels Laboratory, Department of Thermal Energy Engineering, U.S.-Pakistan Centre for Advanced Studies in Energy (USPCAS-E), National University of Sciences & Technology (NUST), Islamabad, Pakistan

²Department of Chemistry, College of Science, University of Hafr Al Batin, Hafr Al Batin, Saudi Arabia

³Chemistry Department, College of Science and Humanities, Prince Sattam bin Abdulaziz University, Alkharj, Saudi Arabia

⁴Department of Chemical Engineering, College of Engineering, King Saud University, Riyadh, Saudi Arabia

⁵The Sargent Centre for Process Systems Engineering, Department of Chemical Engineering, University College London, London, UK

⁶Department of Mechanical Engineering, University of Engineering and Technology, Lahore, Pakistan

⁷Faculty of Engineering, Abu Dhabi University, Abu Dhabi, United Arab Emirates

⁸Institute of Energy and Environmental Engineering, Faculty of Electrical, Energy and Environmental Engineering, University of the Punjab, Lahore, Pakistan

Correspondence

Asif Hussain Khoja, Fossil Fuels Laboratory, Department of Thermal Energy Engineering, U.S.-Pakistan Centre for Advanced Studies in Energy (USPCAS-E), National University of Sciences & Technology (NUST), Sector H-12, Islamabad 44000, Pakistan.

Email: asif@uspcase.nust.edu.pk

Waqar Muhammad Ashraf, The Sargent Centre for Process Systems Engineering, Department of Chemical Engineering, University College London, Torrington Pl, London WC1E 7JE, UK.

Email: waqar.ashraf.21@ucl.ac.uk

Abstract

Copyrolysis, being an active area of research due to its synergistic impact in utilizing diverse fuel resources, including waste materials, like, peach stone (PS), has been the focal point for this study. PS, produced in vast quantities annually and typically intended for landscaping or insulation purposes, is being studied in combination with low-grade bituminous coal for energy utilization focusing on thermokinetics and synergistic aspects. Coal-peach stone (C-PS) blends were formulated at different ratios and subjected to comprehensive characterization techniques, including ultimate analysis (CHN-S), gross calorific value (GCV), Fourier transform infrared spectroscopy, and thermogravimetric analyzer (TGA). The ultimate analysis revealed an enhancement in carbon and hydrogen content from 45.38% to 68.08% and from 3.89% to 6.96%, respectively. Additionally, a reduction in sulfur and nitrogen content from 0.54% to 0.11% and from 1.16% to 0.42%, respectively, was observed with an increase in the ratio of PS in the C-PS blends. The GCV of C-PS blends ranged from 20.75 to 26.01 MJ kg⁻¹. The pyrolysis conditions simulated in TGA are pivotal for evaluating thermokinetics and synergistic effects. The 60C:40PS blend shows a positive synergy index (SI) value of

This is an open access article under the terms of the Creative Commons Attribution License, which permits use, distribution and reproduction in any medium, provided the original work is properly cited.

© 2023 The Authors. *Energy Science & Engineering* published by Society of Chemical Industry and John Wiley & Sons Ltd.

0.0203% concerning total mass loss (ML_T) indicating a favorable condition for bio-oil generation. Coats–Redfern model-fitting method reveals that the activation energy (E_a) of C-PS blends increases in Section II with the addition of PS, and conversely, it decreases in Section III. The E_a for 100PS and 100C was 106.76 and 45.85 kJ mol⁻¹ through (D3) and (F1), respectively, which was improved through the optimal blend 60C:40PS with an E_a of 94.56 and 27.58 kJ mol⁻¹ through (D3) and (F2), respectively. The values obtained from linear regression prove that the kinetic models are effective while the thermodynamic analysis indicates that the pyrolytic behavior of C-PS blends is characterized as endothermic, nonspontaneous, and capable of achieving thermodynamic equilibrium more rapidly.

KEYWORDS

Coats–Redfern model-fitting method, Copyrolysis, Low rank coal, Peach stone, Thermokinetics

1 | INTRODUCTION

Biomass is a viable alternative renewable resource that outperforms other renewable resources in maintaining environmental quality while addressing global energy requirements.¹ Owing to its abundance, renewability, and significant environmental advantages, biomass energy has emerged as one of the most significant sustainable sources of energy, accounting for around 14% of global energy consumption or 38% of that in underdeveloped countries,² biomass holds about 50% of the total renewable energy produced.³ Peach waste is one of the biomass sources which can be used for various energy applications. Due to favorable climatic conditions for peach tree growth, the southern regions of Brazil, Italy, China, Spain, Greece, and the United States are the main producers.^{4,5} On the other hand, 1.5 million hectares of land are harvested to yield nearly 23 million tonnes of peach stone (PS) worldwide.^{6,7} As a result, a substantial amount of nonedible waste is generated during the preparation of these fruits. The PS is produced as agroindustrial waste during the canned peach production process. They account for 10% of the total amount produced by mass, becoming an environmental issue for companies due to a lack of a suitable end destination.⁸

Coal as a fossil fuel is known to be one of the principal energy sources for energy production in many industrialized and developing countries of the world due to escalating energy demands.^{9,10} However, coal usage has implications such as air pollution, which causes various health and environmental challenges, and the rapid global energy consumption of coal, which

contributes to its depletion. These difficulties sparked an exploration of renewable, sustainable, environmentally friendly, and clean energy alternatives. Pyrolysis is a thermochemical process that converts coal and biomass into valuable products, allowing for variable operating conditions and output. It is an endothermic process that produces hydrocarbons in liquid, solid, and gas forms by thermally breaking materials from the exterior to the interior surface.¹ The pyrolysis of coal is inefficient due to the low H/C ratio resulting in significant carbon emissions and low pyrolytic products.¹¹ Although worldwide an energy policy is acceptable to reduce the share of coal as a primary type of fuel in renewable energy, still occupies a prominent spot in power generation in the future because there are some technologies known as coutilization that are developed to provide sensible and ecologically sustainable energy production.¹² One of the primary possibilities for the effective and harmonized use of renewable and fossil energy mix is the co-thermochemical conversion of biomass and coal via copyrolysis. To supply hydrogen for coal, biomass with a higher H/C ratio can be employed.¹³

Previously several investigations have been conducted on the coprocessing of carbonaceous materials, including wheat straw with plastic waste¹⁴ and corn cob with polyethylene.¹⁵ Recently, a multitude of studies has been conducted on the copyrolysis of coal and other biomasses, such as microalgae,¹⁶ sawdust,¹⁷ coconut shell,¹⁸ corn stalks,¹⁹ and corncob.²⁰ Additionally, a number of investigations have been conducted utilizing a thermogravimetric analyzer (TGA) for an in-depth examination of the thermal degradation process during copyrolysis. During copyrolysis, a synergistic effect was

seen at a blend ratio of 30% coal slime and 70% coffee industry residue.²¹ The existence of sufficient hydrogen donors, free ions, and volatile compounds may trigger the synergistic effect because biomass has a greater hydrogen-to-carbon ratio than coal.²² Copyrolysis of biomass and coal tar asphaltene revealed the occurrence of a synergistic effect.²³ The copyrolysis of coal and polyethylene demonstrates how the synergistic effect decreases the copyrolysis activation energy. Additionally, it offered details on the concentrations of hydrogen and hydroxyl ions, which are significant for the interaction mechanisms.²⁴ Several kinetic models have been used to analyze the mechanistic activity of blended samples and their reactivity at various heating rates, blending ratios, and coal and biomass types.²⁵ Designing a pyrolysis system requires careful consideration of the thermokinetic properties.²⁶ The Coats–Redfern (CR) model-fitting method was used to predict the behavior of coal-biomass blends and anticipated reaction pathways, as well as to compute the actual amounts of activation energy (E_a), pre-exponential factor (A), and linear regression (R^2) for every phase of copyrolysis.²⁷ The CR technique evaluates the rationality of multiple models and recommends the best model for coal-biomass blend breakdown. Several studies have investigated the thermal behavior, synergistic effects, and thermokinetic characteristics of coal-biomass copyrolysis.²⁸

The novelty of this study lies in the exploration of a previously uninvestigated area: the copyrolysis of PS with low-rank coal blending. This investigation seeks to elucidate the thermal behavior of these blended materials, necessary energy barriers (required energy input) and operating temperature ranges crucial for the preliminary design of a pyrolysis reactor tailored for the copyrolysis process. While peach stone (100PS) biomass waste is an annual by-product among various available biomasses, its effective energy utilization due to its higher H/C ratio, volatile matter, and availability has not yet been reported with a view to copyrolyse with low-grade coal for more beneficial applications such as bioproducts synthesis instead of the disposal of PS in landfills. To the best of our knowledge, there is no investigation about the synergistic effects and thermokinetics in the copyrolysis of PS with low-rank coal at different blending percentages. Analyzing each feedstock type is crucial in achieving the desired quality and yield in the pyrolysis process. Furthermore, a thorough understanding of the kinetics and overall pyrolysis process is essential for successfully commercializing pyrolysis technology.²⁹ Therefore, the CR model-fitting technique used in this study is presented for the first time to determine the thermokinetic parameters of PS and coal blends during copyrolysis. The most precise kinetic

parameters are predicted based on a higher value of R^2 (0.9–1.0). This work offers helpful insights into the copyrolysis process of PS and coal blends by assessing the synergistic effects coupled with kinetics and thermodynamics parameters. These results may assist in finding the optimal blending ratio for copyrolysis, developing sustainable and environmentally friendly strategies for disposing of waste PS and optimizing the parameters to design copyrolysis reactors.

In this study, the coal-peach stone (C-PS) blends were prepared for the copyrolysis process. The C-PS blends were characterized by ultimate analysis (CHN-S), gross calorific value (GCV), Fourier transform infrared spectroscopy (FTIR), and TGA. The thermal behavior of C-PS blends were assessed using the TGA in an inert (N_2) atmosphere. The difference between experimental and computed data was used to calculate the synergistic effects. The kinetic and thermodynamics characteristics were evaluated by the CR method, which involved the application of eighteen (18) different reaction models. The kinetic and thermodynamic insights reveal the potential of the coutilization of PS in the field of bioenergy production.

2 | EXPERIMENT AND METHODS

2.1 | Materials preparation

For this study, locally collected bituminous coal (100C) and peach stone (100PS) were utilized. Before use, the samples underwent a drying process in the open air for 5 days followed by 1 day in a drier at 105°C to eliminate any remaining moisture, as illustrated in Figure 1. The materials were manually pulverized and sieved automatically in a Sieving WS Tyler RX-29-10 to get the requisite size of 74 μm . Blends were prepared in varying mass ratios of 100:0, 80:20, 60:40, 40:60, 20:80, and 0:100, referred to as 100C, 80C:20PS, 60C:40PS, 40C:60PS, 20C:80PS, and 100PS, respectively. Each blend was homogenized with a vortex mixer for 20 min to ensure homogeneity.

2.2 | Characterization

To assess the proportion of carbon, hydrogen, nitrogen, and sulfur content, the ultimate analyses (CHN-S) were carried out on 100PS, 100C, and their blends. In a CHN analyzer (model; 5ECHN2200-CKIC), the CHN analyses were carried out. Whereas, the sulfur content in the materials was determined by a sulfur analyzer (model; 5EIRS II-CKIC). The 80 mg of each blend and parent

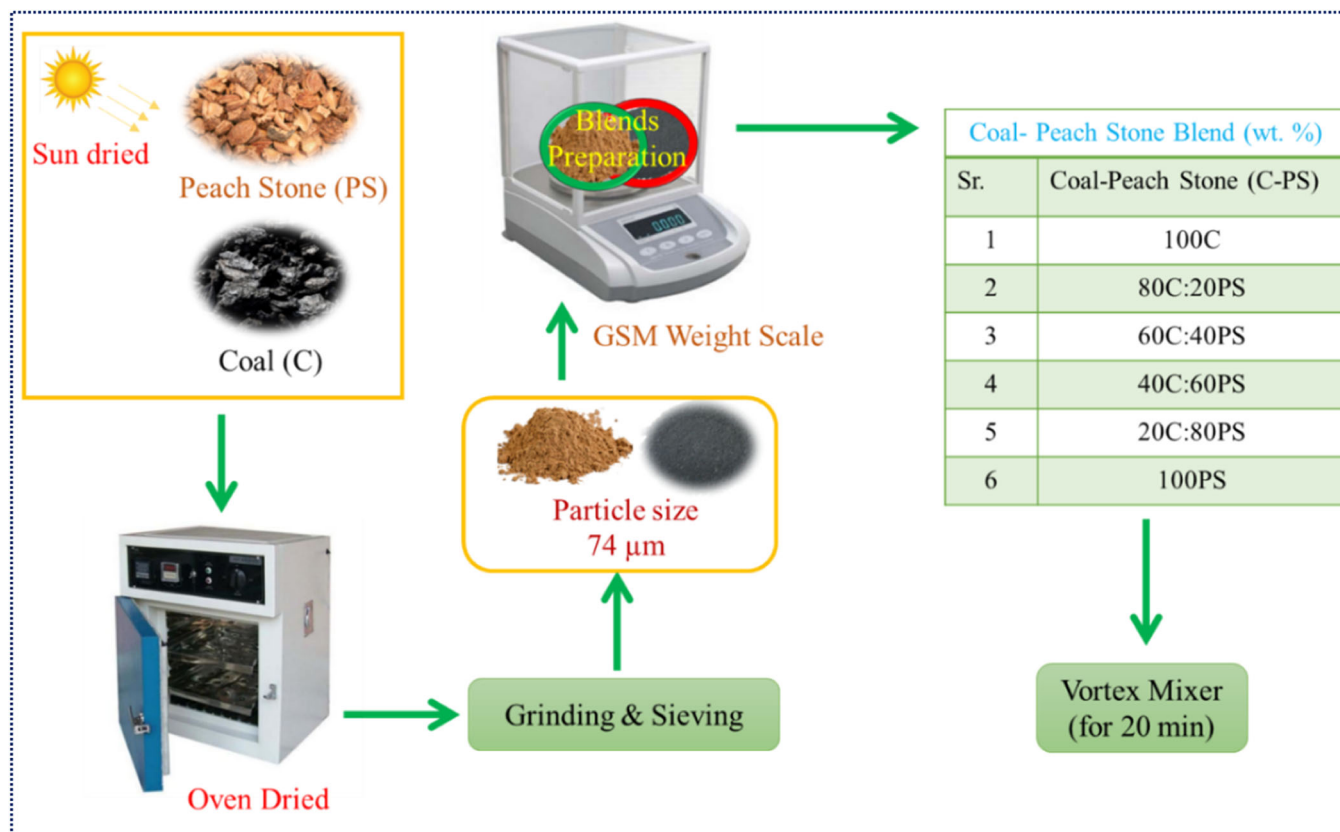


FIGURE 1 Schematic of C-PS blends preparation.

fuels were weighed and put in the aluminum foil. Then, the aluminum foil was placed inside the holder of the analyzer. The CHN composition of the material was determined using helium, nitrogen, and oxygen gases. To assess sulfur content, 300 mg of each sample was placed in a ceramic cup, which was subsequently introduced into the analyzer's furnace. The furnace was set to a temperature of 1350°C, while the oven was maintained at 50°C. Oxygen was introduced into the system at a flow rate of 20 mL min⁻¹. The GCV of each sample was analyzed using the Parr 6200 bomb calorimeter using ASTM D5865-13 standards.

FTIR was conducted in Cary 630, Agilent Technologies to further characterize the chemical bonds present in C-PS blends. The infrared radiation (IR) was directed at each C-PS blend. The IR absorbed by the materials was transformed into vibrational energy and the signals generated will be helpful in the determination of chemical bonding. The absorption range of IR was 650–4000 cm⁻¹ having a resolution of 2 cm⁻¹. The Diamond ATR module was used to perform analysis.

To ascertain the copyrolysis behavior, the TG/DTG analyses of C-PS blends were carried out in TGA 5500 (TA Equipment) at a heating rate of 10°C min⁻¹ at N₂ environment keeping its flow at 35 mL min⁻¹. To

eliminate the systematic error during thermogravimetric (TG), the base experiment was performed thrice to confirm the least variation in the results.

The theoretical value was derived from Equation (1)³⁰ to illustrate the synergistic effect that occurs during the copyrolysis of blends.

$$Y_{th} = X_{PS} \cdot Y_{PS} + X_C \cdot Y_C, \quad (1)$$

where X_{PS} and X_C were the mass ratios of 100PS and 100C, respectively. While Y_{PS} and Y_C were the experimental values obtained from individual pyrolysis of 100PS and 100C, respectively. Furthermore, the synergy index (SI) was calculated from Equation (2),²¹ which provides the presence or absence of interaction and is further helpful in finding the intensity of interaction between C-PS blends, during the copyrolysis process.

$$SI = \frac{Y_{exp} - Y_{th}}{Y_{th}}, \quad (2)$$

where Y_{exp} experimental values were attained during copyrolysis in TG, while Y_{cal} calculated values were obtained using Equation (1).

2.3 | Kinetic and thermodynamics study

The thermal decomposition of C-PS blends was analyzed using reaction kinetic and it helps in deducing the activation energy (Ea), pre-exponential factor (A), and reaction mechanism of solid materials that decompose under specific temperature ranges to produce volatiles and char as described in Equation (3).¹⁷

$$A_{Solid} = B_{Volatiles} + C_{Char}. \quad (3)$$

An accurate way to assess the reaction kinetics for solid-state materials is the CR method. The general CR method kinetic equation is given in Equation (4).³¹

$$\ln \frac{G(\alpha)}{T^2} = \ln \frac{AR}{\beta Ea} \left(1 - \frac{2RT}{Ea} \right) - \frac{Ea}{RT}, \quad (4)$$

where A is the pre-exponential factor (s^{-1}), Ea is the activation energy (kJ mol^{-1}), T is the absolute temperature (K), β is the heating rate ($^{\circ}\text{C min}^{-1}$), $G(\alpha)$ is the kinetic function of various reaction mechanisms, and R ($R = 0.008314 \text{ kJ mol}^{-1} \text{ K}^{-1}$) is the general gas constant.

From Equation (4),³² it was assumed that the expression $-2RT/Ea \ll 1$, so this term is neglected during calculation, Equation (4) simplifies and gives Equation (5).³²

$$\ln \frac{G(\alpha)}{T^2} = \ln \frac{AR}{\beta Ea} - \frac{Ea}{RT}. \quad (5)$$

From the literature, the most common 18 kinetic functions ($G(\alpha)$) were highlighted in Table 1. By plotting a graph between $\ln((G(\alpha))/T^2)$ and $1/T$, a straight line was obtained. After separating the data of the active pyrolysis zone, the linearization of that line was performed, which contributed to finding the intercept and slope of that line. The slope and intercept of the line give Ea and A , respectively. The Ea was calculated from Equation (6),³³ while the A was calculated from Equation (7).³³

$$\text{Slope of line} = -\frac{Ea}{R}, \quad (6)$$

$$\text{Intercept of line} = \ln \frac{AR}{\beta Ea}. \quad (7)$$

The thermodynamic parameters were calculated with the help of experimental data from TG/DTG, along with data on kinetics (Ea and A). The thermodynamic parameters were calculated for parent fuels and each transition zone of the C-PS blend through 18 $G(\alpha)$. This analysis comprises change of enthalpy ΔH (kJ mol^{-1}),

TABLE 1 Kinetic functions $G(\alpha)$ for solid materials thermal decomposition.

Kinetic mechanism	Symbol	$G(\alpha)$	Reference
One and third orders	F1/3	$-3/2[1 - (1 - \alpha)^{2/3}]$	[34]
First order	F1	$-\ln(1 - \alpha)$	[35]
One-and-a-half order	F3/2	$2[(1 - \alpha)^{-1/2} - 1]$	[31, 36]
Second order	F2	$(1 - \alpha)^{-1} - 1$	[36]
Third order	F3	$1/2[(1 - \alpha)^{-2} - 1]$	[37]
Forth order	F4	$1/3[(1 - \alpha)^{-3} - 1]$	[37]
Contracting disk	R1	α	[32]
Contracting cylinder	R2	$1 - (1 - \alpha)^{1/2}$	[37]
Contracting sphere	R3	$1 - (1 - \alpha)^{1/3}$	[38]
Power law	P2	$\alpha^{1/2}$	[28]
Power law	P3	$\alpha^{1/3}$	[28, 29]
Power law	P4	$\alpha^{1/4}$	[28]
Parabolic law	D1	α^2	[32]
Valansi equation	D2	$\alpha + (1 - \alpha)\ln(1 - \alpha)$	[39]
Jander equation	D3	$[(1 - (1 - \alpha)^{1/3})^2]$	[39]
Ginstling-Brounstein equation	D4	$(1 - 2\alpha/3) - (1 - \alpha)^{2/3}$	[40]
Avrami-Erofeev	A2	$(-\ln(1 - \alpha))^{1/2}$	[41]
Avrami-Erofeev	A3	$(-\ln(1 - \alpha))^{1/3}$	[35]

Gibbs-free energy ΔG (kJ mol^{-1}), and entropy ΔS ($\text{kJ mol}^{-1} \text{K}^{-1}$) as presented in Equations (8)–(10).²⁸

$$\Delta H = Ea - RT_p, \quad (8)$$

$$\Delta G = Ea + RT_m \ln(K_b T_p/hA), \quad (9)$$

$$\Delta S = (\Delta H - \Delta G)/T_p, \quad (10)$$

where T_p (K) is the maximum decomposition temperature, K_b ($1.381 \times 10^{-23} \text{ J K}^{-1}$) the Boltzmann constant, and h ($6.626 \times 10^{-34} \text{ J s}$) is the Planks constant.

2.4 | Kinetic and thermodynamics model validation

The kinetic parameters during the thermal degradation of C-PS blends were calculated in two active degradation zones.⁴² The kinetics and thermodynamics were computed using a single-zone approach. This was due to the presence of only one active zone in thermal degradation.

The inputs, outputs, and boundary conditions for calculating kinetic and thermodynamic parameters are presented in Figure 2A,B. First, the TG data were compiled in THINKS_v1.08 software. Then, the kinetic parameters were calculated in MagicPlot3.0 software. The transition zones were determined and their kinetics parameters through each $G(\alpha)$ were obtained. Then, the values of Ea , A , and linear regression (R^2) were extracted from the MagicPlot3.0 to Microsoft Excel for further calculation of thermodynamic parameters. The comparison was made for the specific stage of decomposition of each C-PS blend. The $G(\alpha)$ that showed the highest value for R^2 (0.9–1.0) among all other models was considered the best model that describes the pyrolytic kinetics of C-PS blends.

3 | RESULTS AND DISCUSSION

3.1 | Characterization of materials

The CHN-S analysis was performed to investigate the carbon (C), hydrogen (H), nitrogen (N), and sulfur (S) content present in the C-PS blends as illustrated in Figure 3A–D. The CHN-S analysis was performed not only on parent fuels (100C, 100PS) but also performed for each C-PS blend. The analysis of blends had the goal of determining how blending affected the contents of C, H, N, and S. Figure 3A represents the C content in C-PS blends, it was observed that the C content of 100C was 68.08%, while the C content for 100PS was 45.37%. In the

case of 100C, the coalification process dictates the C content. Specifically, as the coalification processes advance, the carbon content tends to increase.⁴³ The C content within the C-PS blends ranged from 49.69% to 64.92%, achieved through the incorporation of 20%–80% of 100PS biomass. Additionally, it was found that the C content increased with higher proportions of 100C in the blend. It has been reported that homogenized blends possessing compatible properties tend to improve both pyrolytic vapor quality and product quality.⁴⁴

Figure 3B illustrates the H content of 100C (3.89%) and 100PS (6.96%). The higher H content in 100PS signifies that biomass possesses a higher hydrogen content in comparison to coal. This disparity contributes to the increased thermal reactivity of biomass in contrast to coal.⁴⁵ The hydrogen content for C-PS blends ranged from 4.66% to 6.22% which indicates that H content in the blends was increased by the addition of 100PS. Furthermore, the structure of 100C predominantly comprised aromatic C=C rings. These rings were not readily broken at lower pyrolysis temperatures, resulting in lower product yields.⁴³ The higher H content in 100PS, as illustrated in Figure 3B, serves as a hydrogen donor to accelerate the breakdown of 100C during copyrolysis.⁴⁶ The N concentration of C-PS blends is presented in Figure 3C. In comparison to 100PS (with a nitrogen concentration of 0.42%), 100C exhibited a higher nitrogen concentration of 1.16%. However, the N content in C-PS blends ranged from 0.49% to 0.99%. With an increase in the proportion of 100PS in the C-PS blends, the N content demonstrated a reduction. In addition, studies undertaken on NO_x emission during copyrolysis, observed that copyrolysis process has the capability to transform char-bound nitrogen (char-N) into volatile nitrogen (volatile N), potentially leading to a reduction of NO_x emissions.⁴⁷

The S content present in C-PS blends is presented in Figure 3D. It was observed that the S content is mostly found in 100C (0.54%) rather than 100PS (0.11%). The S content within the C-PS blend ranged from 0.19% to 0.45% which indicates that the addition of 100PS in the blends reduces the S content. Additionally, in the copyrolysis of C-PS blends the hydrogen donor nature of 100PS effectively desulfurizes 100C and permits sulfur to release in the form of H_2S .⁴⁸ Hence, copyrolysis of C-PS blends effectively will reduce SO_x emissions. The CHN-S analysis of several coal and biomass feedstocks sourced from the literature is depicted in Table 2. This comparison highlights that the C, H, N, and S content of 100C and 100PS align with the findings reported in the existing literature. The chemical composition of each biomass type is influenced by its distinct climate and formation conditions, thereby leading to alterations in its chemical properties.⁴⁹

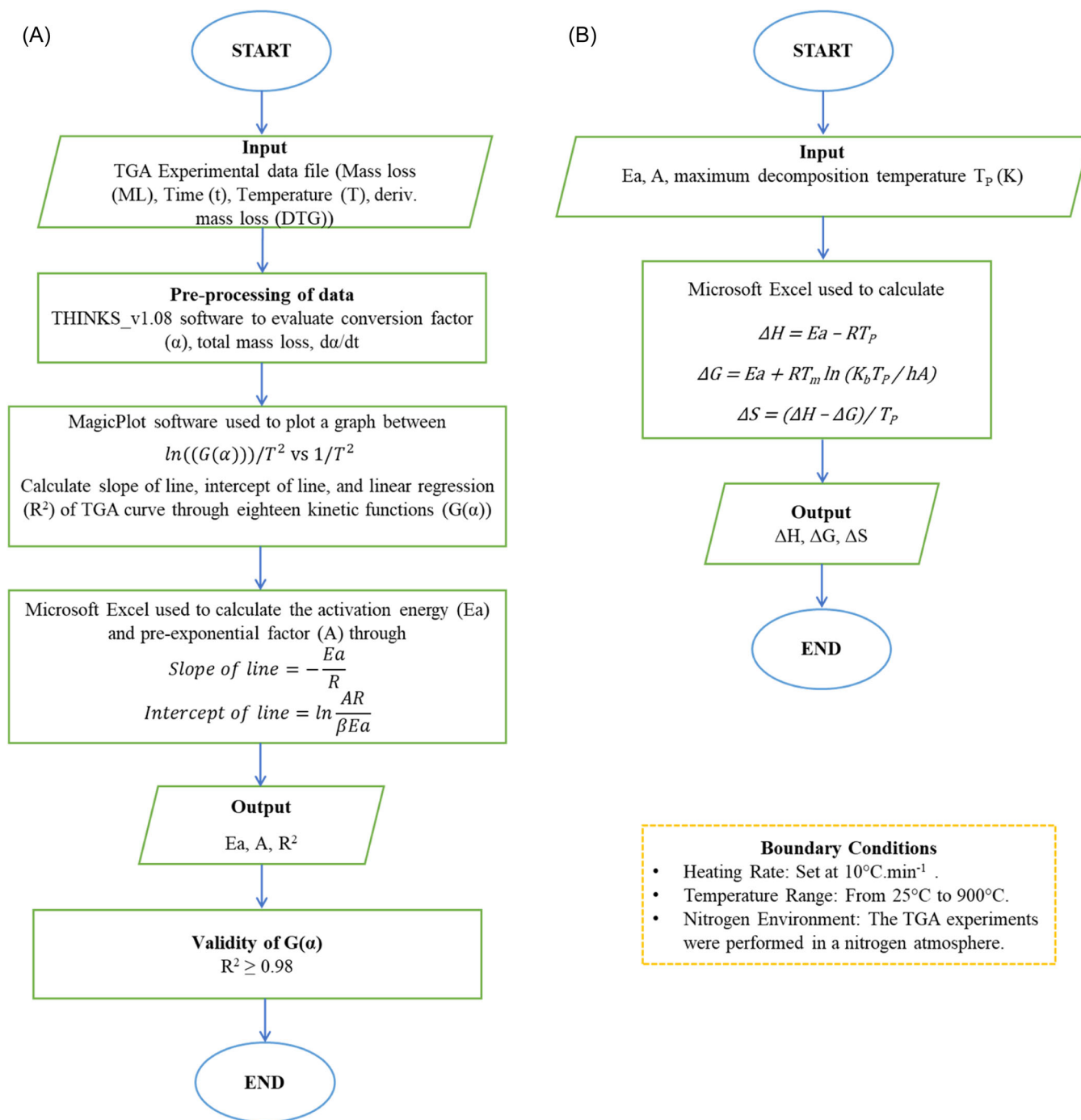


FIGURE 2 Block diagram for calculations of (A) kinetics parameters and (B) thermodynamics parameters. DTG, derivative thermogravimetry; TG, thermogravimetry; TGA, thermogravimetric analysis.

Figure 4 depicts the investigation of the C-PS blends GCV. As could be seen, 100C had a GCV of 27.85 MJ kg^{-1} while 100PS had a GCV of 18.61 MJ kg^{-1} . The GCV for C-PS blends ranged from 20.75 to 26.01 MJ kg^{-1} . The GCV of C-PS blends was greater than individual 100PS. The GCV study of a few coal and biomass feedstocks is presented in Table 2, which demonstrates that the GCV of 100C and 100PS

coincides with the literature. The addition of 100C to C-PS blends enhanced their GCV as a result of the higher C content in 100C, as previously discussed. The GCV of 60C:40PS was 24.03 MJ kg^{-1} which is much better than individual 100PS and also comparable to the energy content of imported fuels considered to be of relatively high quality. As discussed in the ultimate analysis, the C-PS blend coutilization

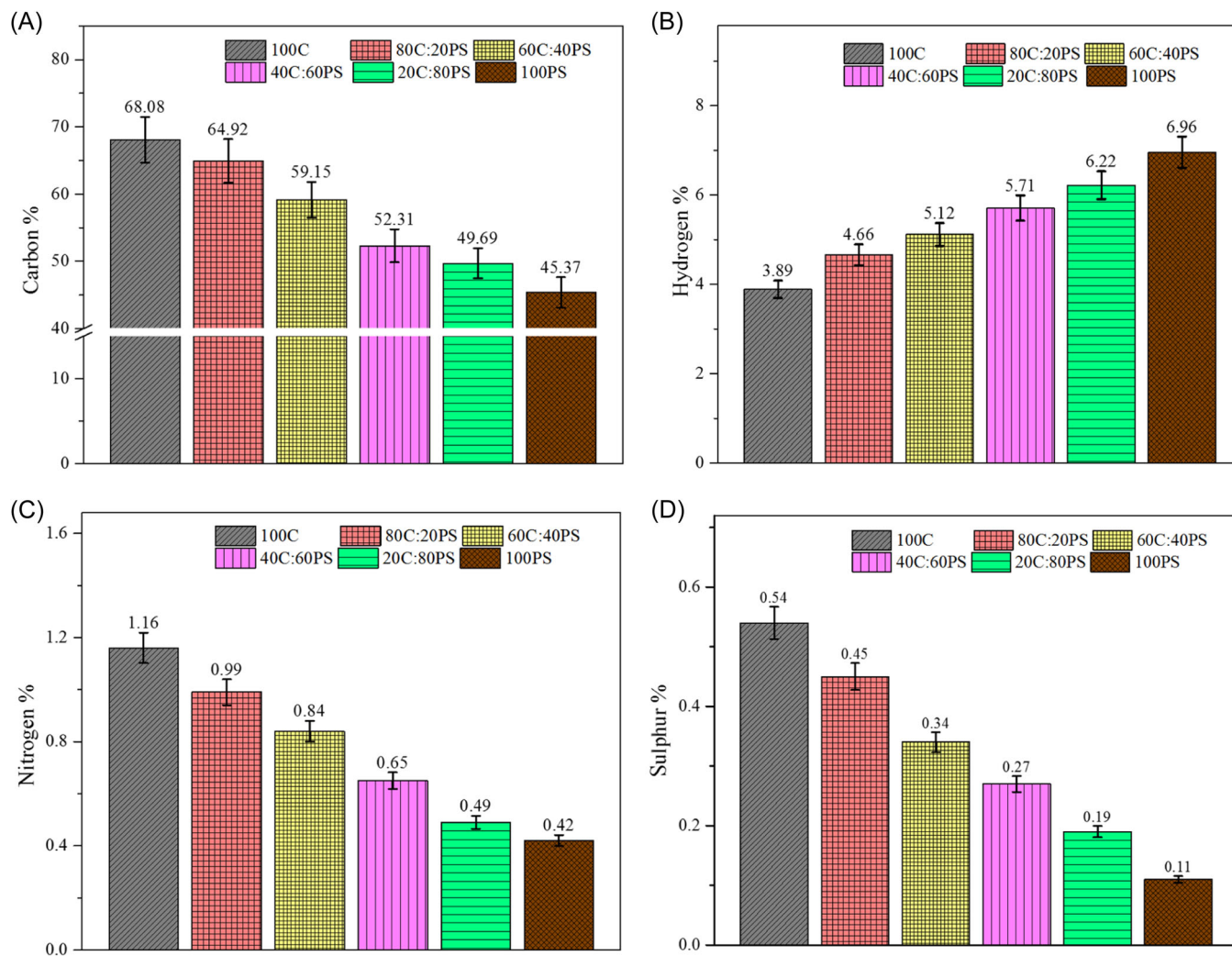


FIGURE 3 Ultimate analysis of C-PS blends (A) carbon, (B) hydrogen, (C) nitrogen, and (D) sulphur content. C-PS, coal-peach stone.

TABLE 2 CHN-S analysis of some coal and biomass feedstock.

Feedstock	Carbon (%)	Hydrogen (%)	Nitrogen (%)	Sulfur (%)	GCV (MJ kg ⁻¹)	Reference
Peach stone (100PS)	45.37	6.96	0.42	0.11	18.61	This study
Peach stone	49.28	6.65	0.34	–	18.379	[6]
Date stone	46.30	6.70	0.83	0.00	16.98	[50]
Hazelnut shell	54.84	5.50	0.44	0.12	19.36	[51]
Peanut shells	47.06	6.07	1.5	0.25	17.05	[36]
Indian almond fruit	50.72	4.98	1.86	0.00	18.31	[52]
Bituminous coal (100C)	68.08	3.89	1.16	0.54	27.85	This study
Fine coal	74.03	5.13	1.04	0.48	28.27	[53]
Bituminous coal, China	61.76	4.16	1.11	0.52	23.526	[54]

Abbreviations: CHN-S, ultimate analysis; GCV, gross calorific value.

reduces the oxygen and hydrogen content while increasing the carbon. Additionally, the copyrolysis of the C-PS blend is expected to lower the emissions of NO_x and SO_x, while raising the GCV.⁴⁴

Figure 5 displays the results of the FTIR analysis for C-PS blends, which reveals the chemical composition of both materials and the resulting blends. The chemical structures of 100C and 100PS contain a variety of

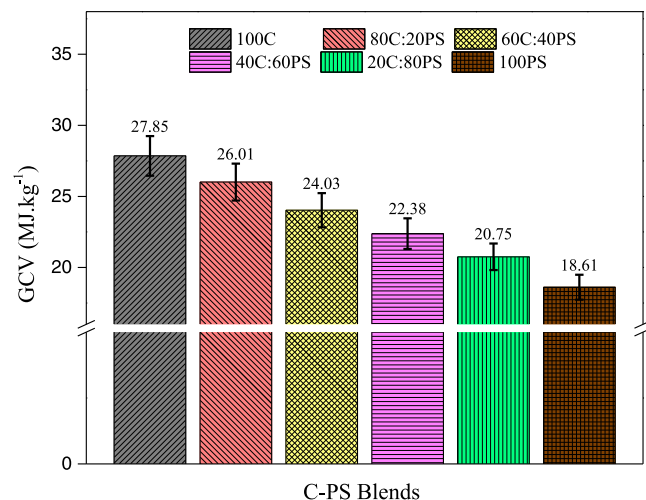


FIGURE 4 GCV analysis of C-PS blends. C-PS, coal-peach stone; GCV, gross calorific value.

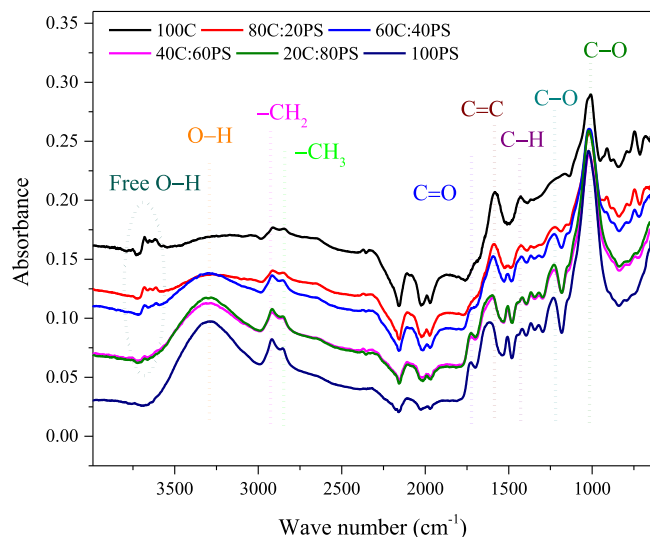


FIGURE 5 FTIR analysis to investigate the chemical structure of C-PS blends. C-PS, coal-peach stone; FTIR, Fourier transform infrared spectroscopy.

functional groups, including O–H, C–H, C=C, and C–O–C. These functional groups indirectly represent the presence of hydrocarbons and identify the extent of their presence by absorbance intensity.⁵⁵ The presence of phenols, alcohols, and organic acids is indicated by the peak for 100C being seen at 3681.0 cm⁻¹ and having a range of 3571.13–3716.56 cm⁻¹ attributed to the free O–H group.⁵⁶ A self-contained hydrogen bond is shown by the peak at 3293.8 cm⁻¹ and its surrounding interval of 3073.94–3531.74 cm⁻¹.⁵⁷ The asymmetric –CH₂ and symmetric –CH₃ stretching vibrations are responsible for the peaks at 2910.65 and 2845.0 cm⁻¹, respectively, and their ranges are 2871.0–2976.77 and 2835.8–2871.1 cm⁻¹,

respectively.⁵⁷ Additionally, the aromatic C=C stretching vibration, which is dominant at 100C, is attributed to the peak at 1578 cm⁻¹ in the range of 1513.78–1670.82 cm⁻¹ as seen in Figure 5. Moreover, the –CH₃ asymmetric deformation vibration is indicated by the minor peak at 1434.89 cm⁻¹ and in the range of 1382.79–1493.6 cm⁻¹. In the range of 1009.90–1127.50 cm⁻¹, another strong peak at 1021.2 cm⁻¹ suggests the presence of C–O stretching vibration.⁵⁸ The peaks identified as the aromatic nucleus between 715.1 and 944.41 cm⁻¹.⁵⁷

The 100PS is mostly composed of three major components hemicellulose, cellulose, and lignin.⁵⁸ The peak observed at 3285.91 cm⁻¹ in a wider range of 2991.92–3678.89 cm⁻¹ specifies the O–H group's stretching vibration due to carbohydrates and lignin.⁵⁹ The peak at 2919.72, 2854.23, and 1422.23 cm⁻¹ in the range of 2874.3–2991.92, 2782.7–2874.3, and 1389.49–1454.98 cm⁻¹ ascribed to the presence of asymmetric –CH₂, symmetric –CH₃, and C–H deformation, respectively.⁵⁸ The presence of an aromatic C=C ring is indicated by the peak at 1612.7 cm⁻¹, which has a range of 1542.06–1697.6 cm⁻¹.⁶⁰ Peaks between 1696.8–1775.02, 1179.60–1291.24, and 833–1179.60 cm⁻¹ are attributable to carbonyl C=O and C–O stretching vibration in esters and ethers bonds, respectively.⁶¹

It further indicates that C-PS blends almost show intermediate behavior of both parent fuels. The intensity of O–H groups was very low in the case of 100C compared with 100PS. This indicates that the O–H groups are mostly found in 100PS. For C-PS blends, the O–H functional group was reduced by increasing the blending ratio of 100C which helped to increase the GCV of blends. Furthermore, the 100C contains fewer aliphatic hydrocarbons (–CH_x) as compared with 100PS. This indicates that hydrogen contents are also high in 100PS as shown previously in CHN-S analysis. The absorbance intensity of the aromatic C=C bond was high in the case of 100C which indicates 100C structure mostly contains carbons as exhibited in the ultimate analysis. Additionally, C-PS blending reduces the intensity of O–H, C=O, aliphatic C–H, C–O–C, and C–O functional groups while increasing the aromatic C=C ring. Hence, reducing the oxygen-holding functional groups and improving the GCV of C-PS blends.

Figure 6 depicts the TG/DTG of C-PS blends copyrolysis. The TG of C-PS blends was conducted at a heating rate of 10°C min⁻¹ to establish effective particle interaction and reduce the amount of inorganic residue after copyrolysis.⁶² The material achieved the target temperature of 900°C more rapidly due to the faster heating rates, ultimately causing a temperature gradient between the material's interior and exterior layers, leading to elevated ignition, peak, and burnout

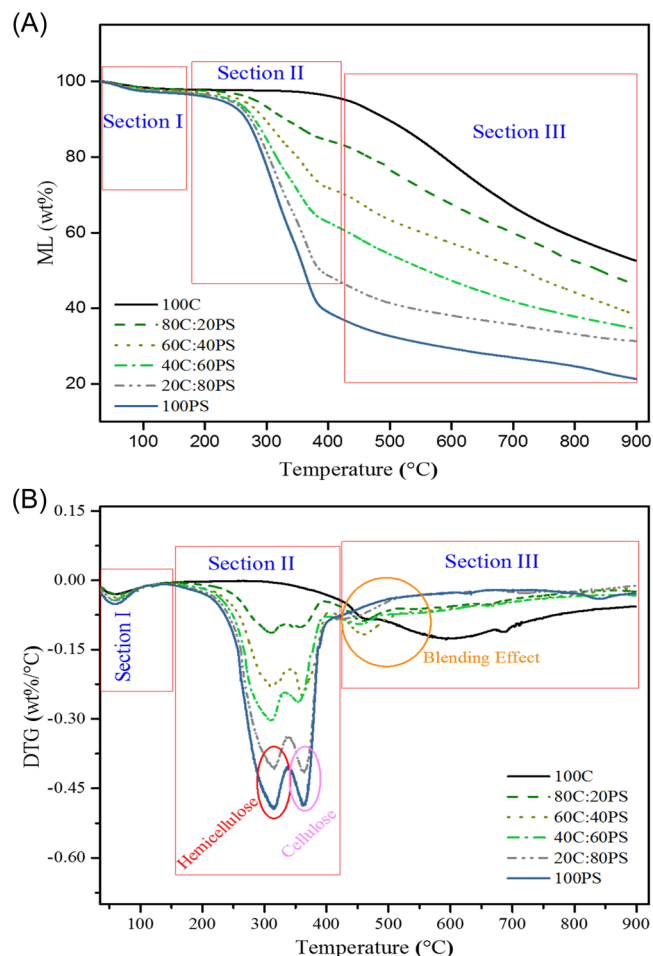


FIGURE 6 TG/DTG copyrolysis of C-PS blends (A) TGA and (B) DTG. C-PS, coal-peach stone; DTG, derivative thermogravimetry; TG, thermogravimetry; TGA, thermogravimetric analysis.

temperatures.⁶³ This phenomenon was explored in the analysis using Figure 6A, illustrating the TG behavior of C-PS blends, and also in Figure 6B, which depicts the derivative thermogravimetry (DTG) patterns of these blends. Due to the higher volatile content in 100PS, there was a notably more substantial mass loss (ML) compared with that observed in 100C. The three parts of the ML of 100PS and 100C are depicted in Figure 6A,B. The evaporation of lighter volatiles and moisture content is represented in the first part, which ranges from 28°C to 146°C. In Section I from Figure 6B, it could be seen that the moisture content was predominantly noticeable in 100PS compared with 100C because bituminous coal contains less moisture than the majority of biomass materials. Section II from Figure 6A,B indicates the active pyrolysis zone, in which most of the volatiles are emitted from 100PS. From Figure 6B, it can be seen that 100PS shows two major peaks for decomposition in Section II. The first peak represents the decomposition of

hemicellulose components (146–338°C), while the second peak in Section II represents the decomposition of cellulose components (338–409.3°C).⁸ The primary thermal decomposition characteristics of Sections II and III are given in Table 2. For 100PS and 100C, the ignition temperature (T_i) was 146°C and 300.4°C, respectively. The T_i for 100PS was less than that for 100C, which shows that 100PS is more reactive than 100C and ignited at much lower temperatures. Lower T_i for 100PS than that for 100C is ascribed to the higher volatile matter present in 100PS.⁶⁴ Moreover, when the T_i of fuel is lower, the fuel will start to decompose at a lower temperature; hence, the reaction requires less energy from an external source and becomes self-sustaining at a lower temperature.⁶⁵ The initiation of reactions at lower temperatures suggests a potential decrease in the energy barrier for these reactions. The final decomposition temperature (T_f) for 100PS and 100C was 409.4°C and 799.8°C, respectively. While the peak decomposition temperature (T_p) for 100PS was 314.2°C and 592.4°C for 100C. It can be seen that the temperature range of thermal decomposition for both 100C and 100PS was different due to the difference in chemical structure. The biomass structure is mainly composed of ether bonds that decompose at a lower temperature, while coal is composed of heavier aromatic C=C bonds that decompose at high temperatures.⁶⁶ The ML in Section II for 100PS was 59.2 wt%, whereas 100C does not have much ML in Section II. The residue left (RL) in Section II for 100PS and 100C was 37.5 and 58.5 wt%, respectively. The maximum decomposition rate (DTG_{max}) for 100PS in Section II was $-0.492 \text{ wt\% } ^\circ\text{C}^{-1}$. Hence, a significant decomposition for 100PS was done in Section II. Section III from Figure 6A,B represents the passive pyrolysis zone that indicates the slow decomposition of lignin and heavier hydrocarbon present in 100PS and 100C, respectively.⁶⁷ The main characteristics of Section III are given in Table 2, which shows there was no peak in Figure 6B observed for the thermal decomposition of 100PS in this section. However, the 100C shows major ML in this section. The ML of 100C in Section III was 38.8 wt%, while the RL and DTG_{max} of 100C were 58.5 wt% and $-0.128 \text{ wt\% } ^\circ\text{C}^{-1}$, respectively.

The copyrolysis behavior for C-PS blends is presented in Figure 6A,B. It could be seen that C-PS blends show three sections for ML. Section I indicates moisture release, Section II reflects the percentage of 100PS in blends, and Section III indicates the ratio of 100C in the blend.⁶⁶ Mostly, the blend behavior was in between the parent fuels as shown in Table 2. Increasing the 100PS blending ratio impacts the T_i , T_f , and T_p for C-PS blends. As could be seen, Section II T_f and T_p underwent very minor changes while the T_i underwent a higher

reduction. The ML and DTG_{max} for C-PS blends increased by the increasing ratio of 100PS in the blend, while the RL exhibited a declining pattern. Section III from Figure 6B shows that T_f was reduced by the addition of 100PS in the blend. The reduction in T_f indicates that the energy consumption for thermal degradation of C-PS blends is becoming low as compared with individual coal.

Table 2 shows that the total mass loss (ML_T) and total residue left (RL_T) after 900°C in 100C were 47.61 and 52.39 wt%, respectively. ML_T and RL_T for 100PS were 78.81 and 21.8 wt% which is almost consistent with the literature.⁸ The ML_T and RL_T for C-PS blends were in the range of 53.75–68.87 and 31.13–46.25 wt%, respectively. The ML_T for C-PS blends increased by raising the 100PS ratio in the blends, while RL_T for blends decreased.

Synergistic and inhibitory effects in C-PS blends were investigated through Equation (1). The computed values derived from Equation (2) were compared with the experimental values of ML_T and RL_T , as revealed in Table 3. A positive value of the SI in terms of ML_T indicates the presence of synergistic effect, whereas the negative values show an inhibitory effect.⁶⁸ Figure 7A represents the synergistic evaluation in terms of TG analysis, while Figure 7B shows the DTG representation of the synergistic effect. From Figure 7A,

It could be seen that the synergistic effect or inhibitory effect was not prominent before 400°C which might be due to the reflection of 100PS in the blend. After 400°C the synergistic effect was detected from the temperature 400–650°C that is due to the emission of volatiles from 100PS which help in the thermal cracking of 100C. As a result, for this specific temperature range, the experimental ML_T of blends is much greater than the estimated values. Figure 7B shows that the T_i , T_f , and T_p of the C-PS blend are also altered by adding 100PS and 100C, indicating the synergistic effect. At high temperatures (600–900°C), the alkaline earth metals present in biomass can absorb SO_x , like, sulfites and sulfates, which provide a reduction in SO_x emissions.⁴⁷ Table 3 presents the SI in terms of ML_T and RL_T during copyrolysis which shows the presence and intensity of synergistic or inhibitory effects. It was observed that the blend 60C:40PS shows a positive value (0.0203 wt%) in terms of ML_T while showing a negative value (−0.0303 wt%) in terms of RL_T indicating the presence of a synergistic effect in this blend.⁶⁹ The difference in values shows the volatile–volatile reaction and volatile–char reactions.⁷⁰ Additionally, the other blends 80C:20PS, 40C:60PS, and 20C:80PS show the negative value (−0.0018, −0.0171, and −0.0509 wt%, respectively) in terms of ML_T that refers to the inhibitory effect. The synergistic effect in

TABLE 3 TG/DTG thermal decomposition characteristics of C-PS blends (Sections II and III).

Characteristics	100C	80C:20PS	60C:40PS	40C:60PS	20C:80PS	100PS
<i>Section II</i>						
T_i (°C)	–	179.5	163.9	156.2	151.9	146
T_p (°C)	–	310.8	309.0	312.0	315.7	314.2
T_f (°C)	–	397.2	401.7	402.4	406.6	409.4
ML (wt%)	–	13.0	26.5	34.7	49.3	59.2
RL (wt%)	–	84.3	71.0	62.4	48.0	37.8
DTG_{max} (wt% °C ^{−1})	–	−0.112	−0.227	−0.304	−0.409	−0.492
<i>Section III</i>						
T_i (°C)	300.4	397.2	401.7	402.4	406.6	–
T_p (°C)	592.4	458.2	459.1	458.2	435.6	–
T_f (°C)	799.8	531.0	518.7	486.0	483.8	–
ML (wt%)	38.8	10.83	9.10	7.15	5.90	–
RL (wt%)	58.5	62.6	61.9	55.2	42.1	–
DTG_{max} (wt% °C ^{−1})	−0.128	−0.089	−0.118	−0.096	−0.082	–
<i>Overall (25–900°C)</i>						
ML_T (wt%)	47.61	53.75	61.31	65.19	68.87	78.81
RL_T (wt%)	52.39	46.25	38.69	34.81	31.13	21.18

Abbreviations: C-PS, coal-peach stone; DTG, derivative thermogravimetry; ML, mass loss; RL, residue left; TG, thermogravimetry.

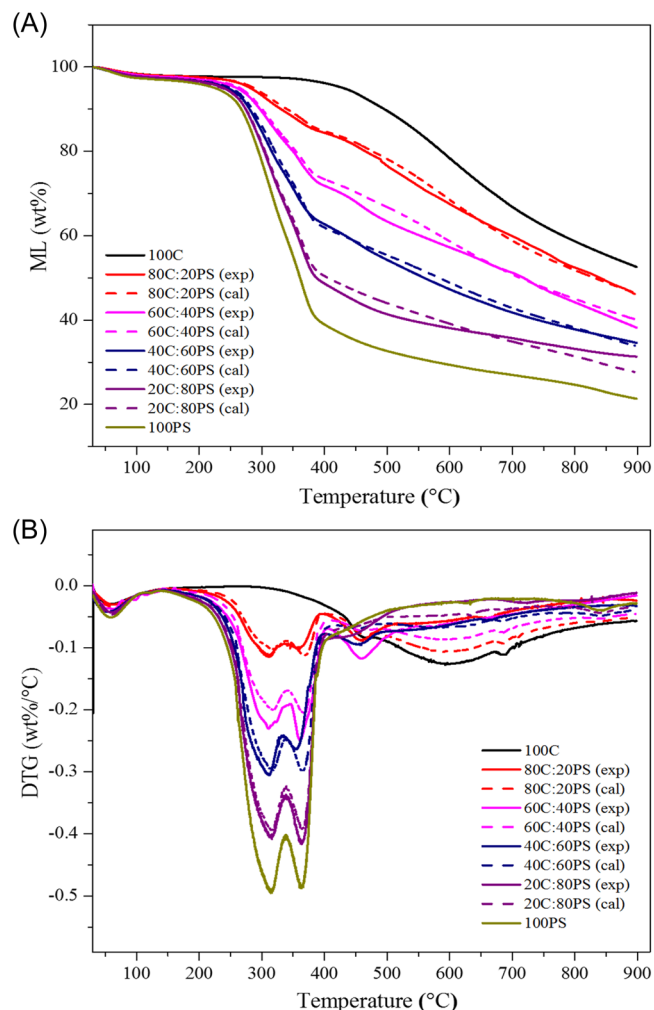


FIGURE 7 Synergistic effect investigation on C-PS blends (A) TGA curves and (B) DTG curves. C-PS, coal-peach stone; DTG, derivative thermogravimetry; ML, mass loss; TGA, thermogravimetric analysis.

C-PS blends may result from the transfer of H and OH radicals from 100PS to 100C, which accelerates the thermal cracking of 100C, and due to the presence of alkali and alkaline earth metals.⁶⁰ Therefore, it is suggested that the blending ratio of 60C:40PS should be adopted (at $10^{\circ}\text{C min}^{-1}$) to gain a synergistic effect.

3.2 | Kinetics and thermodynamics analysis

The thermokinetic characteristic of C-PS blends was investigated by employing the CR method. To compute the consequences of the blending ratio on the copyrolysis characteristics, 18 kinetic functions ($G(\alpha)$) were executed.³⁴ The kinetic parameters E_a , A , and R^2 were extracted from TG/DTG statistics data and presented in

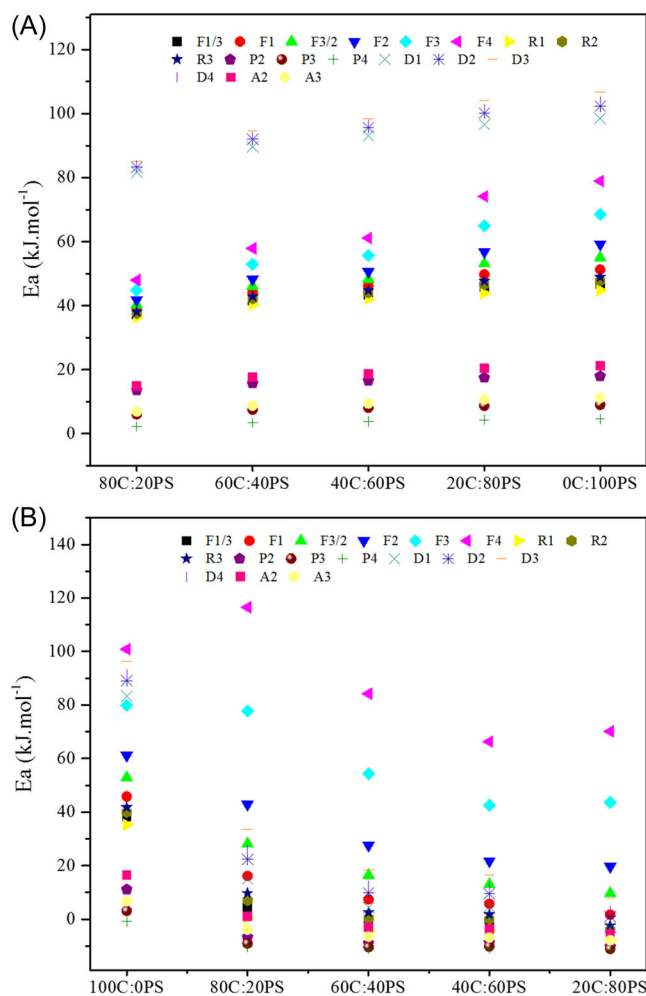


FIGURE 8 E_a of C-PS blends through 18 kinetic functions $G(\alpha)$: (A) Section II and (B) Section III. C-PS, coal-peach stone.

Supporting Information Table S1. The E_a of C-PS blends through 18 $G(\alpha)$ were computed and illustrated in Figure 8A,B. The moisture content sections of C-PS blends were not included in the kinetics study because kinetic parameters have a negligible or small influence on the overall process in this section. The kinetics characteristics were calculated in Sections II and III from Figure 6A,B. Also, the temperature range for the kinetic study was adopted from Table 2. The primary ML for 100PS occurred in Section II and was termed an active pyrolysis zone since the reaction occurred owing to the breakdown of hemicellulose and cellulose in this zone.⁷¹ While for 100C the main pyrolysis zone was Section III because major ML occurred in this section. For C-PS blends, there were two major zones of thermal degradation Sections II and III. Figure 8A represents the E_a during thermal decomposition in Section II, while Figure 8B shows the E_a during Section III. From Figure 8A,B and Supporting Information Table S1, it was perceived that the E_a and A for 100PS were more

than 100C through all $G(\alpha)$. While for C-PS blends, it could be seen that the E_a and A were lowest for 80C:20PS in Section II, among all other blends. In Section II, the highest values of E_a and A for each C-PS blend were obtained through the Jander diffusion equation (D3) as revealed in Figure 8A. The D3 model shows high values of E_a in Section II that was 106.76, 104.25, 98.40, 94.56, and 85.15 kJ mol⁻¹ while the A was 1.4×10^7 , 7.2×10^6 , 1.2×10^6 , 4.8×10^5 , and 3.3×10^4 s⁻¹ for 100%, 80%, 60%, 40%, and 20% of PS in the blend, respectively. Figure 8A shows that the lowest values of E_a and A were obtained from the power law equation (P4). Conferring to the P4 model the E_a for 100%, 80%, 60%, 40%, and 20% of PS was 4.54, 4.30, 3.87, 3.42, and 2.28 kJ mol⁻¹, while the A was 0.028, 0.025, 0.020, 0.016, and 0.007 s⁻¹, respectively. In Section III, Figure 8B shows that the highest E_a and A were obtained through a fourth-order chemical reaction (F4), while the E_a and A for 100%, 80%, 60%, 40%, and 20% of coal in the blend were 100.90, 116.55, 84.19, 66.24, and 70.10 kJ mol⁻¹, and 1.2×10^6 , 9.6×10^7 , 1.9×10^6 , 6.9×10^5 , and 1.1×10^6 s⁻¹, respectively. The lowest values of E_a and A were obtained through the P4 model in Section III. The literature presented on copyrolysis of date palm seeds and cashew shell waste revealed that the chemical reaction (CRO3) model produced high values of E_a for blends containing 100%, 50%, and 0% of date palm seeds, respectively. These values were recorded as 186.05, 187.35, and 197.23 kJ mol⁻¹. In contrast, the nucleation reaction (NM3) model displayed the lowest values of E_a , which were measured as 2.30, 2.67, and 3.94 kJ mol⁻¹ for blends containing 100%, 50%, and 0% of date palm seeds, respectively.²⁷ Furthermore, in another copyrolysis study of biochar derived from sewage sludge and lignin, the 3-D-J (Jander) model showed high values of E_a in Stages 2 and 3. The E_a in Stage 2 was 96.65, 86.91, 81.75, 73.97, and 69.05 kJ mol⁻¹ for 100%, 80%, 60%, 40%, and 20% of sewage sludge biochar in the blend. While the lowest values of E_a in both stages of that study were obtained by reaction order (F0).⁷² Some of the $G(\alpha)$ show negative values of E_a as shown in Supporting Information Table S1 which indicates this $G(\alpha)$ was not suitable for defining the copyrolysis behavior of C-PS blends.⁶⁶ The values of parameter A provide insights into the structure of the material. Lower values are indicative of surface reactions, while higher value refers to the complex reaction.⁶⁹ Consequently, the higher value of E_a and A for 100PS indicates that the chemical reaction is more complicated. Whereas at a higher A value, the E_a was also observed to be high and vice versa.⁷³

The thermodynamic characteristics of C-PS blends were derived from the kinetics study. The calculations for thermodynamics parameters are presented in Supporting

Information Table S2. The thermodynamics parameters obtained from 18 $G(\alpha)$ are shown in Figure 9A–F. The T_p was taken from Table 2 for Sections II and III. The ΔH values for C-PS blends were higher in Section II than the values obtained from Section III for all $G(\alpha)$ as depicted in Figure 9A,B. In Section II, positive ΔH shows the reaction is endothermic.⁷⁴ While in Section III, the ΔH values were negative and positive, as shown in Supporting Information Table S2, indicating the reaction is endothermic and exothermic.³⁴ The values of ΔG were positive in both Sections II and III as shown in Figure 9C,D which indicates the reaction is nonspontaneous.⁷⁵ Whereas as per Figure 9E,F, ΔS displays negative values in both Sections II and III, indicating that the structure of C-PS blends was more ordered.⁷⁶

3.3 | Thermokinetic model validation

The behavior of coal and biomass blends during pyrolysis and combustion is often assessed using just first-order chemical reactions (F1).⁷⁷ In this study, the most common 18 $G(\alpha)$ from Table 1 was used to examine the kinetic mechanism of C-PS blends for each stage of decomposition. The objective of using 18 $G(\alpha)$ is to determine the best response mechanism for each stage of C-PS blends. The comparison in 18 $G(\alpha)$ was made based on higher R^2 .⁷⁸ The $G(\alpha)$ was thought to be the best model to describe the kinetics and thermodynamics during copyrolysis since it demonstrates the best convergence of data sets.⁷⁹ For each $G(\alpha)$ and C-PS blend during Sections II and III, Supporting Information Table S1 displays the value of R^2 . Figure 10A–F represents the best-fitted $G(\alpha)$ that was based on a higher value of R^2 . From Figure 10A, it can be seen that the F1 model for 100C shows the highest value of R^2 (0.9931) among all other $G(\alpha)$. In Section III, the E_a and A for 100C were 45.85 kJ mol⁻¹ and 25.945 s⁻¹, respectively. For 100PS the highest value of R^2 (0.9873) was obtained from the Jander diffusion equation (D3) as shown in Figure 10B. The corresponding E_a and A for 100PS were 106.76 kJ mol⁻¹ and 1.44×10^7 s⁻¹. The E_a values in a study of the pyrolysis of hazelnut, walnut, and pistachio shells were 60.9, 69.6, and 73.5 kJ mol⁻¹, respectively.⁵¹ Additionally, Table 7 displays that the 100PS and 100C kinetic and thermodynamic parameters estimated using the CR approach are in good agreement with the findings given in the literature. The variation in E_a during the pyrolysis of biomass and coal is caused by a number of variables, including the inert gas used for pyrolysis, the heating rate, the reaction mechanism, and the particle size of sample.⁸⁰ For C-PS blends in Section II, the highest R^2 values (0.982–0.987) were obtained

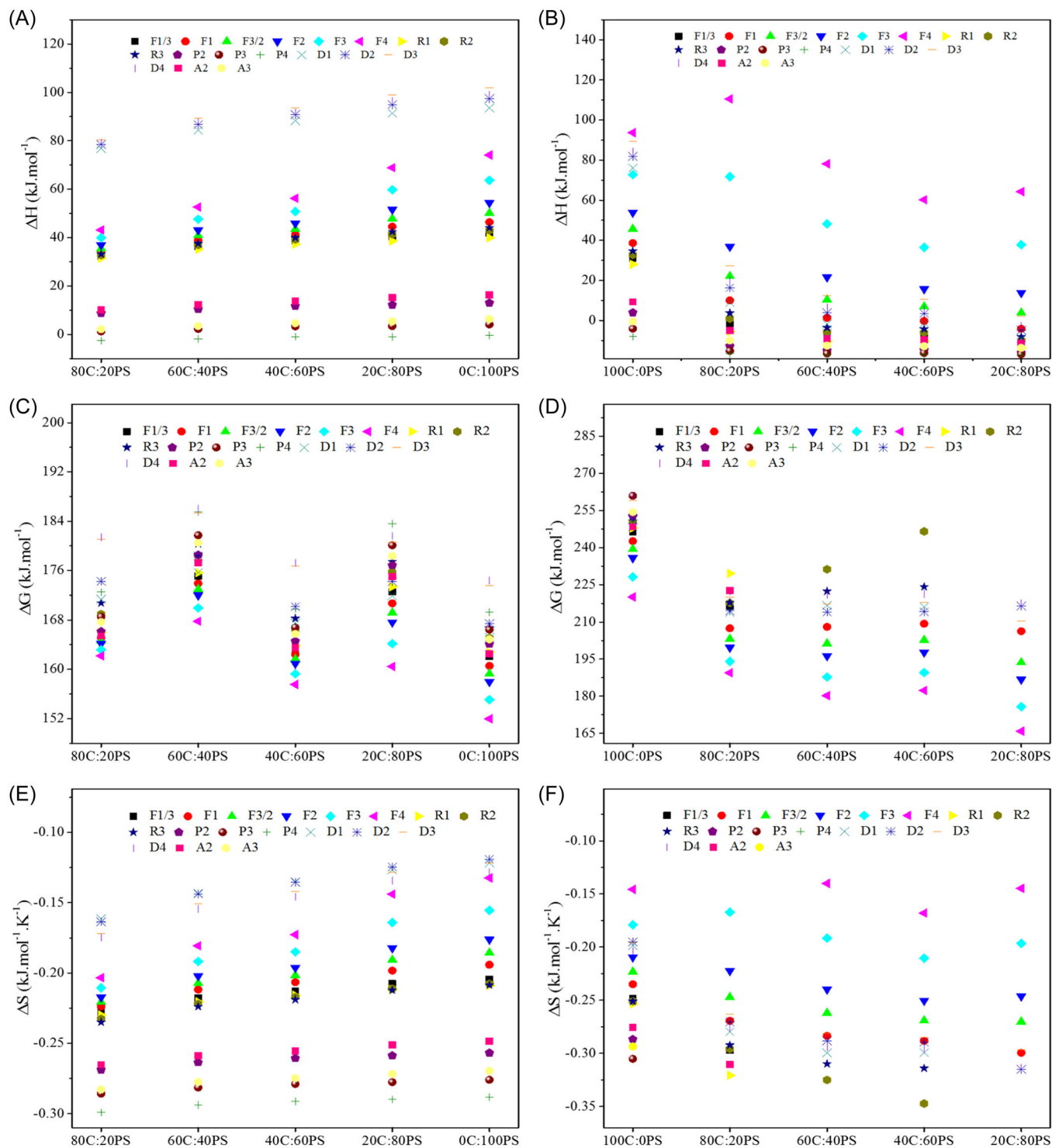


FIGURE 9 Thermodynamic parameters of C-PS blends (A) ΔH , Section II, (B) ΔH , Section III, (C) ΔG , Section II, (D) ΔG , Section III, (E) ΔS , Section II, and (F) ΔS , Section III. C-PS, coal-peach stone.

from the D3 model as shown in Figure 10C–F. The E_a and A was 85.15, 94.56, 98.40, and 104.25 $\text{kJ}\cdot\text{mol}^{-1}$ and 3.37×10^4 , 4.87×10^5 , 1.29×10^6 , and 7.22×10^6 s^{-1} , respectively, for 80%, 60%, 40%, and 20% coal in the blend. It was observed that the E_a and A for C-PS blends in Section II were increased by the augment of PS in the

blend. The findings of kinetic parameters evaluated for C-PS blends are consistent with recent literature presented in Table 7. In copyrolysis of *Miscanthus sacchariflorus* and three different rank coals, authors note that raising the biomass percentage in the blend raises the E_a of the blend.⁸¹ The E_a obtained based on a

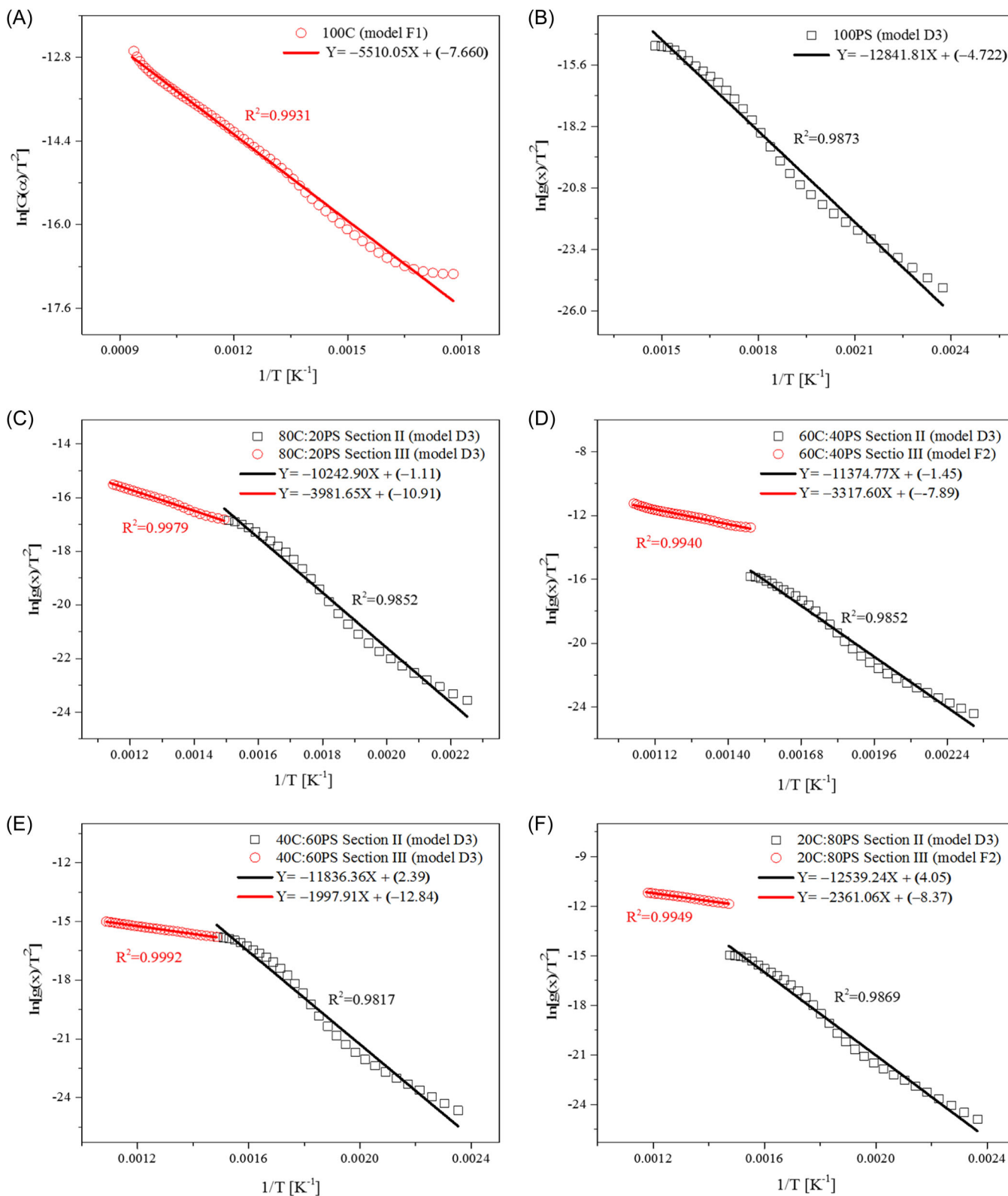


FIGURE 10 Model fitted with highest R^2 for C-PS blends (A) 100C, (B) 100PS, (C) 80C:20PS, (D) 60C:40PS, (E) 40C:60PS, and (F) 20C:80PS. C-PS, coal-peach stone.

higher value of R^2 for each section of C-PS blends is illustrated in Figure 11 and the kinetics characteristics were presented in Table 4. In Section III from Table 4, it can be seen that the C-PS blend shows different models for the highest R^2 . The 80C:20PS and 40C:60PS blends show the highest value of R^2 (0.998–0.999) through the D3 model. While, the E_a and A were 33.49 and 16.61 kJ mol^{-1} , at 0.763 and 0.052 s^{-1} for 80% and 60% coal in the blend, respectively. 60C:40PS and 80C:20PS in Section III show a higher value of R^2 (0.994–0.995) through the second-order chemical reaction (F2). The E_a of 60C:40PS and 80C:20PS was 27.58 and 19.62 kJ mol^{-1} , whereas the value of A was 12.373 and 5.440 s^{-1} , respectively. For C-PS blends, Table 4 indicates that the E_a and A in Section III were lower by adding PS to the blends. Hence, adding PS to the blends is useful to reduce the E_a in Section III⁶⁶ as illustrated in Figure 11. This finding substantiates that blended fuels in the post-425°C temperature range will require the selection of a short period of residence time

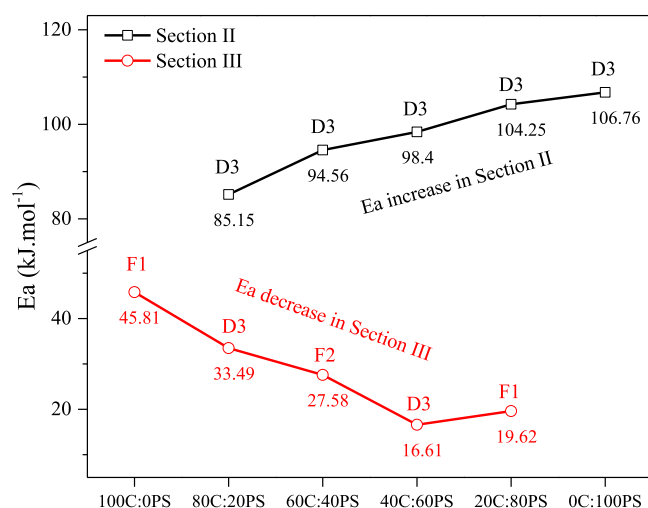


FIGURE 11 E_a of C-PS blends in Sections II and III having the highest R^2 values. C-PS, coal-peach stone.

while designing a copolymer reactor for biofuel production.

The thermodynamics parameter of verified models is presented in Table 5. The ΔH values for 100C and 100PS were 38.59 and 101.88 kJ mol^{-1} , respectively, which shows that both individual fuels are endothermic and require an external energy source to produce biofuels.⁷⁵ For C-PS blends the ΔH values in Section II were in the range of 80.29–98.96 kJ mol^{-1} . While in Section III the ΔH values ranged from 13.79 to 27.34 kJ mol^{-1} . Table 5 demonstrates how the percentage of PS in the blend causes the ΔH to rise in Section II and behave oppositely in Section III, indicating that the ΔH and E_a behave similarly during copyrolysis.⁶⁶ Furthermore, the difference between E_a and ΔH for each C-PS blend was less than 6 kJ mol^{-1} , indicating a decreased energy barrier and the viability of biofuel production.⁸²

The ΔG values for 100C and 100PS were 242.63 and 173.52 kJ mol^{-1} , respectively, and show positive values that indicate 100C is more nonspontaneous than 100PS.⁷⁵ Section II for C-PS blends shows that the ΔG values are in the range of 176.76–185.34 kJ mol^{-1} . While in Section III, the ΔG values were 186.77–220.01 kJ mol^{-1} as shown in Table 5 confirming that less energy from an external source will be required in making the activated complex. It is also notable that ΔG values for the blends in both sections (Sections II and III) were less than 100C which also indicates that 100C requires less energy from an external source to make an activated complex.⁷⁶ The ΔS values for 100C and 100PS were -0.235 and -0.122 $\text{kJ mol}^{-1} \text{K}^{-1}$. The ΔS for C-PS blends in Section II was in the range of -0.128 to -0.172 $\text{kJ mol}^{-1} \text{K}^{-1}$. While Section III was -0.240 to -0.285 $\text{kJ mol}^{-1} \text{K}^{-1}$. Table 6 shows that in Section II the ΔS values decreased with increasing the PS in the blend. While in Section III the vice versa trend was observed. The lower value of ΔS for 100C indicates lower activity and takes more time to move towards thermodynamic equilibrium as compared

Sample	Experimental		Calculated		Synergy index (SI)	
	ML_T (wt%)	RL_T (wt%)	ML_T (wt%)	RL_T (wt%)	ML_T (wt%)	RL_T (wt%)
100C	47.61	52.39	–	–	–	–
80C:20PS	53.75	46.25	53.85	46.14	–0.0018	0.0023
60C:40PS	61.31	38.69	60.09	39.90	0.0203	–0.0303
40C:60PS	65.19	34.81	66.33	33.66	–0.0171	0.0341
20C:80PS	68.87	31.13	72.57	27.42	–0.0509	0.1353
100PS	78.81	21.18	–	–	–	–

TABLE 4 Synergistic effect investigation on major characteristics from TG/DTG.

Abbreviations: DTG, derivative thermogravimetry; ML, mass loss; RL, residue left; TG, thermogravimetry

TABLE 5 Kinetic characteristics of C-PS blends copyrolysis after selection of the best model.

Parameters	100C	80C:20PS	60C:40PS	40C:60PS	20C:80PS	100PS
<i>Section II</i>						
$G(\alpha)$	–	D3	D3	D3	D3	D3
E_a (kJ mol ⁻¹)	–	85.15	94.56	98.40	104.25	106.76
A (s ⁻¹)	–	3.37×10^4	4.87×10^5	1.29×10^6	7.22×10^6	1.44×10^7
R^2	–	0.985	0.985	0.982	0.987	0.987
<i>Section III</i>						
$G(\alpha)$	F1	D3	F2	D3	F2	–
E_a (kJ mol ⁻¹)	45.81	33.49	27.58	16.61	19.62	–
A (s ⁻¹)	25.945	0.763	12.373	0.052	5.440	–
R^2	0.993	0.998	0.994	0.999	0.995	–

Abbreviation: C-PS, coal-peach stone.

TABLE 6 Thermodynamic characteristics of C-PS blends copyrolysis after selection of the best model.

Parameters	100C	80C:20PS	60C:40PS	40C:60PS	20C:80PS	100PS
<i>Section II</i>						
ΔH (kJ mol ⁻¹)	–	80.29	89.27	93.53	98.96	101.88
ΔG (kJ mol ⁻¹)	–	181.08	185.34	176.70	180.57	173.52
ΔS (kJ mol ⁻¹ K ⁻¹)	–	–0.172	–0.151	–0.142	–0.128	–0.122
<i>Section III</i>						
ΔH (kJ mol ⁻¹)	38.59	27.34	21.52	10.56	13.79	–
ΔG (kJ mol ⁻¹)	242.63	220.01	196.26	217.88	186.77	–
ΔS (kJ mol ⁻¹ K ⁻¹)	–0.235	–0.263	–0.240	–0.285	–0.246	–

Abbreviation: C-PS, coal-peach stone.

with 100PS.⁸³ The thermodynamic parameters evaluated for 100C and 100PS are consistent with the literature as presented in Table 7. The higher value of ΔS in conjunction with lower values of E_a and A for the blends, in post 425°C operating temperature (Section III) signifies fast reactions with a relatively shorter time to reach thermodynamic equilibrium. According to the thermokinetics model-fitted study, C-PS blends are suitable for boosting bioenergy production and successfully turning PS waste into a useful product, the 60C:40PS blend showed optimal results and is favoring its selection via SI for bio-oil production.

3.4 | Impact of properties of C-PS blends on the thermokinetics

This section discusses the influence of physiochemical aspects on thermokinetics. In-depth analyses of 100C and

100PS were carried out, and the results are compared with existing research in Table 1. When 100C and 100PS were compared with different coals and biomasses, the present study revealed that 100PS had the greatest hydrogen concentration, nearly 7%, while having the lowest carbon content (45%) that is also being verified in terms of the value of GCV (18.61 MJ kg⁻¹). In 100PS biomass, nitrogen and sulfur were discovered to be present in amounts less than 0.5%. This indicates that when mixing 100PS with 100C, less harmful gases, such as sulfur oxides and nitrogen oxides, will develop. The GCV of 100C, which is 27.85 MJ kg⁻¹, is validated by the average carbon percentage of almost 68%, however, the hydrogen percentage is the lowest at 3.89%. The hydrogen content of 100PS is higher than that of 100C since the GCV reduces with oxygen content and increases with carbon and hydrogen concentrations.⁵² Additionally, in both 100C and 100PS, the ML_T at Stage I was lower than that of Stages II and III. This shows that

TABLE 7 Kinetic and thermodynamic parameters of coal and biomass calculated using Coats–Redfern method.

Feedstock	Best-fitted model	E_a (kJ mol ⁻¹)	ΔH (kJ mol ⁻¹)	ΔG (kJ mol ⁻¹)	ΔS (kJ mol ⁻¹ K ⁻¹)	Reference
Peach stone (100PS), Bituminous coal (100C)	Jander equation-diffusion models (D3), and First-order-chemical reaction (F1)	100PS = 106.76, 100C = 45.81	100PS = 101.88, 100C = 38.59	100PS = 173.52, 100C = 242.63	100PS = -0.122, 100C = -0.235	This study
Date seeds (DS), Cashew shells (CS)	Ginstling-Brounstein, Jander, and Ginstling equations-diffusion models	DS = 104–118, CS = 115–134	DS = 102–116, CS = 112–132	DS = 150–156, CS = 161–168	DS = -0.13 to -0.16, CS = -0.11 to -0.14	[27]
Hemp (H), sawdust (SD), sub-bituminous coal (C)	Deceleratory reaction mechanism (R3), second- order chemical reaction (F2), and one-and- a-half chemical reaction (F3/2)	H = 44, SD = 60, C = 39	H = 39, SD = 55, C = 33	H = 160, SD = 176, C = 201	H = -0.197, SD = -0.187, C = -0.227	[66]
Rice husk (RH), bituminous coal (C)	Chemical reaction order 1 (F ₁), and chemical reaction order 1.5 (F _{1.5})	RH = 59.15–67, C = 25.28–30.64	RH = 53.89–62.54, C = 19.20–24.56	RH = 443.5–445.7, C = 525.9–527.9	RH = -0.603 to -0.620, C = -0.685 to -0.695	[60]
Date palm surface fibers	Diffusion models (one-way transport [DM1], and Valensi equation [DM4])	84–100	80–97	151–164	-0.17 to -0.18	[84]
Algae consortium (AC), low-rank coal (BC)	Jander equation-diffusion models (D3), and third-order-chemical reactions (F3)	AC = 78.22, BC = 85.04	AC = 73.44, BC = 78.99	AC = 170.70, BC = 197.10	AC = -0.17, BC = -0.16	[85]

neither of them significantly lost mass up to 146°C, proving that they are both thermally stable in Stage I and that the C-PS blends performed similarly. In general, the mass losses resulting from the individual pyrolysis of both 100PS and 100C are not equal to the ML_T recorded during the copyrolysis of both materials. This indicates that copyrolysis entails interactions between the specific decomposition processes associated with each feedstock. Several studies have demonstrated that copyrolysis of biomass and coal produces an SI, which ultimately lowers the E_a of the reactions and increases the yield of volatiles while also lowering the temperature at which the maximum weight loss rate occurs,⁸⁶ so that interactions may arise through chemical reactions and physical action. The SI is significantly reduced at higher temperatures (>700°C) since most volatiles have been released and there are no longer any discernible interactions with blended solid residues.⁴³ The pace at which chemical reactions take place under reaction circumstances is known as the kinetic study. This study's kinetic analysis shows that a material's physiochemical characteristics influence its chemical reactions. The intricate multistep processes involved in the thermal breakdown of C-PS blends indicate that the process is not a straightforward one, and the pyrolysis mechanisms of 100C and 100PS differed. When 100C is compared with 100PS pyrolysis, the average E_a in copyrolysis was thus greatly lowered by blends. Lower E_a indicated that the addition of biomass was beneficial for 100C pyrolysis since E_a is an energy barrier that must be overcome for the chemical reaction to proceed. Owing to the interactions of radicals formed from 100C and 100PS, the 60C:40PS mix proved to be the most effective, making it more reactive and decomposable.⁸⁷ In comparison to the 100C, the ΔH readings for the 100PS were noticeably greater. Nevertheless, ΔH reduces when 100C and 100PS are pyrolyzed in equal parts, especially for the optimal blend of 60C:40PS. Energy-efficient systems benefit from reduced ΔH . Different thermodynamic characteristics may be used to evaluate different feedstocks and shed light on the viability and spontaneity of the chemical reactions involved.⁴⁶

In light of the findings, it is recommended to operate the full-scale copyrolyser reactor between 425°C and 700°C, particularly for the examined blend, with special attention to the 60C:40PS blend. This recommendation stems from several factors including the reduced time required to achieve thermodynamic equilibrium, the positive SI, decreased energy from an external source (energy barrier), and the potential interactions of radicals. The outcomes of this research confirm that 100PS biomass would make a suitable candidate for copyrolysis, thereby serving as a possible source of bioenergy.

4 | CONCLUSIONS

The present study revealed that copyrolysis of PS, a waste material utilized effectively instead of disposal after peach utilization in industries, and bituminous coal outperform the pyrolysis of individual materials in terms of evaluating its SI, thermokinetics, and reaction mechanism. The TGA results indicate that the ML_T for 100PS and 100C were 78.81% and 47.61%, respectively. This confirms a higher presence of volatiles in 100PS and with its increasing ratio within C-PS blends, the ML_T also increases ranging from 53.75% to 68.87%. Furthermore, the SI of 0.0203% was observed only in the 60C:40PS blend, pertaining to the ML_T recorded at 61.31%. This occurrence indicates a positive effect conducive to the bio-oil generation, while, an inhibitory effect was observed for the remaining C-PS blends in terms of ML_T favoring the bio-char formation. To comprehend the thermokinetic properties of C-PS blends, the CR model-fitting method with 18 kinetic functions was applied. The E_a for 100PS and 100C was 106.76 and 45.85 kJ mol⁻¹ through D3 and F1 reaction mechanistic models, respectively. In Section II, the E_a of C-PS blends increased with the incorporation of 100PS. Conversely, in Section III, the opposite trend was observed, where the addition of 100PS led to a decrease in E_a . For C-PS blends, in Section II the kinetic study reveals the D3 model while, in Section III, F2, and D3 models were observed to be most suitable for accurately defining the copyrolysis reaction mechanism. The optimized blend, 60C:40PS, lowered the E_a of the base fuels to 94.56 and 27.58 kJ mol⁻¹, as determined by the D3 and F2 models, respectively, in both sections of this study. The optimized blend showed a preference for selection based on the SI suitable for the purpose of bio-oil production. The positive values of ΔH and ΔG for C-PS blends indicate that the copyrolysis reactions were endothermic and nonspontaneous showing feasibility under specific conditions. The values of ΔH and ΔG were also optimized through the optimal blend 60C:40PS to 89.27 and 185.34 kJ mol⁻¹ in Section II and 21.52 and 196.26 kJ mol⁻¹ in Section III, respectively. While the ΔS shows negative values which indicates the reaction is nearer to accomplishing its thermodynamics equilibrium and stable product formation in copyrolysis of 100C and 100PS. The results obtained from this in-depth thermokinetic study are crucial for the efficient design of a copyrolysis system for bioenergy production. An important recommendation inferred from this study is to operate the full-scale copyrolyser reactor within the temperature range of 425–700°C, particularly for the 60C:40PS blend. This approach when adopted shortens the duration required to attain thermodynamic

equilibrium, diminishes reliance on external sources (reduced energy barrier), and enhances interactions amongst radicals due to the increased presence of volatiles. This operational strategy is expected to increase the efficacy and efficiency of the copyrolysis process, especially for the generation of bio-oil; nevertheless, further investigations are necessary to use these by-products for commercial-level applications with minimum up-gradation.

CONFLICT OF INTEREST STATEMENT

The authors declared no conflict of interest.

ORCID

Asif Hussain Khoja  <http://orcid.org/0000-0002-9006-3456>

Waqar Muhammad Ashraf  <http://orcid.org/0000-0003-1841-7659>

M. A. Mujtaba  <http://orcid.org/0000-0001-9134-9002>

Fahid Riaz  <http://orcid.org/0000-0002-6468-614X>

REFERENCES

1. Pritam K, Puppala H, Palla S, Suriapparao DV, Basak T. A two-step hybrid multi-criteria approach to analyze the significance of parameters affecting microwave-assisted pyrolysis. *Process Saf Environ Prot.* 2023;171:975-985.
2. Tiwari A, Marella TK. Algal biomass: potential renewable feedstock for biofuel production. In: Srivastava N, Srivastava M, Mishra P, Gupta V, eds. *Substrate analysis for effective biofuels production.* Clean energy production technologies. 2020. Springer. https://doi.org/10.1007/978-981-32-9607-7_1
3. Walia A, Putatunda C, Solanki P, Pathania S, Bhatia RK. Co-conversion of algal biomass to biofuel. *Liquid Biofuels: Fundamentals, Characterization, and Applications.* 2021; 391-439. [doi:10.1002/9781119793038.ch11](https://doi.org/10.1002/9781119793038.ch11)
4. Sousa SDF, da Silva FB, de Araújo AC, Gomes JP. Determinação das propriedades físicas e físico-químicas de pêssegos cultivar Rubimel. *Rev Bras Tecnol Agroind.* 2018;12(2). [doi:10.3895/rbta.v12n2.7166](https://doi.org/10.3895/rbta.v12n2.7166)
5. Smykov A, Mesyats Ny. State Analysis of Horticulture and Peach Culture in the World. In: *Plant Biol Hortic Theory Innov. NBG – NSC Russia.* 155:130-137. [doi:10.36305/2712-7788-2020-2-155-130-137](https://doi.org/10.36305/2712-7788-2020-2-155-130-137)
6. Özsın G, Pütün AE. A comparative study on co-pyrolysis of lignocellulosic biomass with polyethylene terephthalate, polystyrene, and polyvinyl chloride: synergistic effects and product characteristics. *J Clean Prod.* 2018;205: 1127-1138.
7. Fao F. Agriculture Organization of the United Nations; 2016.
8. Valadão LS, Dos Santos Duarte C, de Los Santos DG, Filho PJS. Conversion of peach endocarp and polyethylene residue by the co-pyrolysis process. *Environ Sci Pollut Res.* 2022;29(7):10702-10716.
9. Magida NE, Bolo LL, Hlangothi SP, Dugmore G, Ogunlaja AS. Co-combustion characteristics of coal-*Scenedesmus* microalgae blends and their resulting ash. *Combust Sci Technol.* 2021;193(3):419-436.

10. Martins F, Felgueiras C, Smitková M. Fossil fuel energy consumption in European countries. *Energy Procedia*. 2018;153:107-111.
11. Nyoni B, Duma S, Bolo L, Shabangu S, Hlangothi SP. Co-pyrolysis of South African bituminous coal and *Scenedesmus* microalgae: kinetics and synergistic effects study. *Int J Coal Sci Technol*. 2020;7(4):807-815.
12. Larionov KB, Mishakov IV, Slyusarskiy KV, et al. Combustion of bituminous coal and semicoke with copper salts. *Fuel Process Technol*. 2021;213:106706.
13. Wu Z, Zhang J, Fan Y, et al. Synergistic effects from co-pyrolysis of lignocellulosic biomass with low-rank coal: a perspective based on the interaction of organic components. *Fuel*. 2021;306:121648.
14. Singh S, Tagade A, Verma A, Sharma A, Tekade SP, Sawarkar AN. Insights into kinetic and thermodynamic analyses of co-pyrolysis of wheat straw and plastic waste via thermogravimetric analysis. *Bioresour Technol*. 2022;356:127332.
15. Singh S, Patil T, Tekade SP, Gawande MB, Sawarkar AN. Studies on individual pyrolysis and co-pyrolysis of corn cob and polyethylene: thermal degradation behavior, possible synergism, kinetics, and thermodynamic analysis. *Sci Total Environ*. 2021;783:147004.
16. Wu Z, Yang W, Tian X, Yang B. Synergistic effects from co-pyrolysis of low-rank coal and model components of microalgae biomass. *Energy Convers Manage*. 2017;135:212-225.
17. Bhattacharyya M, Shadangi KP, Mahanta P, Mohanty K. Co-pyrolysis of coal-biomass: study on reaction kinetics and thermodynamics. *Biofuels Bioprod Biorefin*. 2022;16(3):725-742. doi:10.1002/bbb.2333
18. Adewole BZ, Adeboye BS, Malomo BO, Obayopo SO, Mamuru SA, Asere AA. Co-pyrolysis of bituminous coal and coconut shell blends via thermogravimetric analysis. *Energy Sources Part A: Recovery Util Environ Effects*. 2020;1-14. doi:10.1080/15567036.2020.1798567
19. Chen X, Liu L, Zhang L, et al. Thermogravimetric analysis and kinetics of the co-pyrolysis of coal blends with corn stalks. *Thermochim Acta*. 2018;659:59-65.
20. Xue Y, Guo H, Lei Y, Wang M, Liu F. Synergy effects of the co-pyrolysis of coal and corncob on sulfur transformation under different atmospheres. *J Therm Anal Calorim*. 2022;147:8985-8995.
21. Ni Z, Bi H, Jiang C, et al. Investigation of the co-pyrolysis of coal slime and coffee industry residue based on machine learning methods and TG-FTIR: synergistic effect, kinetics and thermodynamic. *Fuel*. 2021;305:121527.
22. Wu L, Liu J, Xu P, Zhou J, Yang F. Biomass hydrogen donor assisted microwave pyrolysis of low-rank pulverized coal: optimization, product upgrade and synergistic mechanism. *Waste Manage*. 2022;143:177-185.
23. Zhou R, Cao R, Liu Y, et al. Study on the characteristics and mechanism of fast co-pyrolysis of coal tar asphaltene and biomass. *J Anal Appl Pyrolysis*. 2022;161:105409.
24. Hong D, Li P, Si T, Guo X. ReaxFF simulations of the synergistic effect mechanisms during co-pyrolysis of coal and polyethylene/polystyrene. *Energy*. 2021;218:119553.
25. Verma K, Gajera ZR, Sawarkar AN. Kinetics of gasification and co-gasification of petcoke and coal. *J Inst Eng (India): Ser E*. 2022;103(1):31-39.
26. Saeed S, Saleem M, Durrani A. Thermal performance analysis and synergistic effect on co-pyrolysis of coal and sugarcane bagasse blends pretreated by trihexyltetradecylphosphonium chloride. *Fuel*. 2020;278:118240.
27. Raza M, Abu-Jdayil B. Synergic interactions, kinetic and thermodynamic analyses of date palm seeds and cashew shell waste co-pyrolysis using Coats-Redfern method. *Case Stud Therm Eng*. 2023;47:103118.
28. Florentino-Madiedo L, Vega MF, Díaz-Faes E, Barriocanal C. Evaluation of synergy during co-pyrolysis of torrefied sawdust, coal and paraffin. A kinetic and thermodynamic study. *Fuel*. 2021;292:120305.
29. Raza M, Abu-Jdayil B, Inayat A. Pyrolytic kinetics and thermodynamic analyses of date seeds at different heating rates using the Coats-Redfern method. *Fuel*. 2023;342:127799.
30. Liu X, Burra KRG, Wang Z, Li J, Che D, Gupta AK. Towards enhanced understanding of synergistic effects in co-pyrolysis of pinewood and polycarbonate. *Appl Energy*. 2021;289:116662.
31. Raza M, Abu-Jdayil B, Al-Marzouqi AH, Inayat A. Kinetic and thermodynamic analyses of date palm surface fibers pyrolysis using Coats-Redfern method. *Renewable Energy*. 2022;183:67-77.
32. Postawa K, Fałynowicz H, Szczygieł J, Beran E, Kułażyński M. Analyzing the kinetics of waste plant biomass pyrolysis via thermogravimetry modeling and semi-statistical methods. *Bioresour Technol*. 2022;344:126181.
33. Santos Santana M, Pereira Alves R, da Silva Borges WM, Francisquini E, Guerreiro MC. Hydrochar production from defective coffee beans by hydrothermal carbonization. *Bioresour Technol*. 2020;300:122653.
34. Naqvi SR, Hameed Z, Tariq R, et al. Synergistic effect on co-pyrolysis of rice husk and sewage sludge by thermal behavior, kinetics, thermodynamic parameters and artificial neural network. *Waste Manage*. 2019;85:131-140.
35. Singh RK, Patil T, Verma A, Tekade SP, Sawarkar AN. Insights into kinetics, reaction mechanism, and thermodynamic analysis of pyrolysis of rice straw from rice bowl of India. *Bioresour Technol Rep*. 2021;13:100639.
36. Açıklan K. Determination of kinetic triplet, thermal degradation behaviour and thermodynamic properties for pyrolysis of a lignocellulosic biomass. *Bioresour Technol*. 2021;337:125438.
37. Subramanian S, Ragula UBR. Kinetics of catalytic and non-catalytic pyrolysis of *Nerium oleander*. *Fuel*. 2020;280:118591.
38. Jiang L, Zhang D, Li M, et al. Pyrolytic behavior of waste extruded polystyrene and rigid polyurethane by multi kinetics methods and Py-GC/MS. *Fuel*. 2018;222:11-20.
39. Li J, Dou B, Zhang H, Zhang H, Chen H, Xu Y. Thermochemical characteristics and non-isothermal kinetics of camphor biomass waste. *J Environ Chem Eng*. 2021;9(4):105311.
40. Du J, Dou B, Zhang H, et al. Non-isothermal kinetics of biomass waste pyrolysis by TG-MS/DSC. *Carbon Capture Sci Technol*. 2023;6:100097.
41. Mian I, Li X, Jian Y, et al. Kinetic study of biomass pellet pyrolysis by using distributed activation energy model and Coats Redfern methods and their comparison. *Bioresour Technol*. 2019;294:122099.

42. Liu X, Chen M, Wei Y. Kinetics based on two-stage scheme for co-combustion of herbaceous biomass and bituminous coal. *Fuel*. 2015;143:577-585.
43. Wang W, Lemaire R, Bensakhria A, Luat D. Review on the catalytic effects of alkali and alkaline earth metals (AAEMs) including sodium, potassium, calcium and magnesium on the pyrolysis of lignocellulosic biomass and on the co-pyrolysis of coal with biomass. *J Anal Appl Pyrolysis*. 2022;163:105479.
44. Bhattacharyya M, Shadangi KP, Mahanta P, Mohanty K. Co-pyrolysis of coal-biomass: study on reaction kinetics and thermodynamics. *Biofuels Bioprod Biorefin*. 2022;16(3):725-742.
45. Kumar PS, Edwin M, Percy AJ. Comparative study on pyrolysis characteristics and kinetics of Indian almond fruit and *Gracilaria changii* seaweed by thermogravimetric analysis. *Biomass Convers Biorefin*. 2022;1-16. doi:10.1007/s13399-022-03662-z
46. Zhang P, Chen Z, Zhang Q, Zhang S, Ning X, Zhou J. Co-pyrolysis characteristics and kinetics of low metamorphic coal and pine sawdust. *RSC Adv*. 2022;12(34):21725-21735.
47. Li L, Liu G, Li Y, et al. Release of sulfur and nitrogen during co-pyrolysis of coal and biomass under inert atmosphere. *ACS Omega*. 2020;5(46):30001-30010.
48. Quan C, Gao N. Copyrolysis of biomass and coal: a review of effects of copyrolysis parameters, product properties, and synergistic mechanisms. *BioMed Res Int*. 2016;2016:1-11.
49. Vassilev SV, Vassileva CG, Vassilev VS. Advantages and disadvantages of composition and properties of biomass in comparison with coal: an overview. *Fuel*. 2015;158:330-350.
50. Parthasarathy P, Fernandez A, Singh DK, et al. Thermogravimetric analysis of camel dung, date stone, and their blend for pyrolytic, kinetic, and thermodynamic studies. *Cleaner Chem Eng*. 2022;4:100072.
51. Melikoglu M, Ozdemir M, Ates M. Pyrolysis kinetics, physicochemical characteristics and thermal decomposition behavior of agricultural wastes using thermogravimetric analysis. *Energy Nexus*. 2023;11:100231.
52. Suresh Kumar P, Edwin M, Bensam Raj J. Pyrolysis characteristics and kinetic analysis of Indian almond fruit biomass by thermogravimetric analysis for the potential source of bioenergy. *Proc Inst Mech Eng Part E: J Process Mech Eng*. 2022;237(2):290-299.
53. Aprianti N, Faizal M, Said M, Nasir S, Fudholi A. Gasification kinetic and thermodynamic parameters of fine coal using thermogravimetric analysis. *Energy*. 2023;268:126666. doi:10.1016/j.energy.2023.126666
54. Li G, Chen Z, Wu A, et al. Pyrolysis and co-combustion of semi-dry sewage sludge and bituminous coal: kinetics and combustion characteristics. *Catalysts [Online]*. 2022.
55. Kumar P, Nandi BK. Effect of rice husk and petroleum coke blending on combustion characteristics of high ash Indian coals. *Biomass Convers Biorefin*. 2023;13:13065-13079. doi:10.1007/s13399-021-02090-9
56. Dun W, Guijian L, Ruoyu S, Xiang F. Investigation of structural characteristics of thermally metamorphosed coal by FTIR spectroscopy and X-ray diffraction. *Energy Fuels*. 2013;27(10):5823-5830.
57. Jiang J, Zhang S, Longhurst P, Yang W, Zheng S. Molecular structure characterization of bituminous coal in Northern China via XRD, Raman and FTIR spectroscopy. *Spectrochim Acta Part A*. 2021;255:119724.
58. Chen X, Liu L, Zhang L, Zhao Y, Qiu P. Pyrolysis characteristics and kinetics of coal-biomass blends during co-pyrolysis. *Energy Fuels*. 2019;33(2):1267-1278.
59. Chutia RS, Katak R, Bhaskar T. Thermogravimetric and decomposition kinetic studies of *Mesua ferrea* L. deoiled cake. *Bioresour Technol*. 2013;139:66-72.
60. Tauseef M, Ansari AA, Khoja AH, et al. Thermokinetics synergistic effects on co-pyrolysis of coal and rice husk blends for bioenergy production. *Fuel*. 2022;318:123685.
61. Gupta S, Gupta GK, Mondal MK. Slow pyrolysis of chemically treated walnut shell for valuable products: effect of process parameters and in-depth product analysis. *Energy*. 2019;181:665-676.
62. Elkhailifa S, Mariyam S, Mackey HR, Al-Ansari T, McKay G, Parthasarathy P. Pyrolysis valorization of vegetable wastes: thermal, kinetic, thermodynamics, and pyrogas analyses. *Energies*. 2022;15(17):6277.
63. Escalante J, Chen W-H, Tabatabaei M, et al. Pyrolysis of lignocellulosic, algal, plastic, and other biomass wastes for biofuel production and circular bioeconomy: a review of thermogravimetric analysis (TGA) approach. *Renewable Sustainable Energy Rev*. 2022;169:112914.
64. Garcia E, Ejim IF, Liu H. Thermogravimetric analysis of co-combustion of a bituminous coal and coffee industry by-products. *Thermochim Acta*. 2022;715:179296.
65. Basu P. Chapter 3—Biomass characteristics. In: Basu P, ed. *Biomass Gasification, Pyrolysis and Torrefaction*. 2nd ed. Academic Press; 2013:47-86.
66. Gohar H, Khoja AH, Ansari AA, et al. Investigating the characterisation, kinetic mechanism, and thermodynamic behaviour of coal-biomass blends in co-pyrolysis process. *Process Saf Environ Prot*. 2022;163:645-658.
67. Laougé ZB, Merdun H. Investigation of thermal behavior of pine sawdust and coal during co-pyrolysis and co-combustion. *Energy*. 2021;231:120895.
68. Merdun H, Laougé ZB, Çığgın AS. Synergistic effects on co-pyrolysis and co-combustion of sludge and coal investigated by thermogravimetric analysis. *J Therm Anal Calorim*. 2021;146(6):2623-2637.
69. Merdun H, Laougé ZB. Kinetic and thermodynamic analyses during co-pyrolysis of greenhouse wastes and coal by TGA. *Renewable Energy*. 2021;163:453-464.
70. Zhang J, Yang H, Kang G, et al. The synergistic effect on the product distribution for the co-pyrolysis of tannery wastes. *Fuel*. 2022;322:124080.
71. Narnaware SL, Panwar NL. Kinetic study on pyrolysis of mustard stalk using thermogravimetric analysis. *Bioresour Technol Rep*. 2022;17:100942.
72. Dai Q, Xiang W, Liu Q, Wang M, Zhang X. Co-pyrolysis biochar derived from sewage sludge and lignin: synergetic effect and adsorption properties. *J Environ Chem Eng*. 2022;10(3):107898.
73. Singh B, Singh S, Kumar P. In-depth analyses of kinetics, thermodynamics and solid reaction mechanism for pyrolysis of hazardous petroleum sludge based on isoconversional models for its energy potential. *Process Saf Environ Prot*. 2021;146:85-94.

74. Huang L, Liu J, He Y, et al. Thermodynamics and kinetics parameters of co-combustion between sewage sludge and water hyacinth in CO₂/O₂ atmosphere as biomass to solid biofuel. *Bioresour Technol.* 2016;218:631-642.
75. Hu Y, Liu J, Li X, et al. Assessment of the pyrolysis kinetics and mechanism of vegetable-tanned leathers. *J Anal Appl Pyrolysis.* 2022;164:105502.
76. Ni Z, Bi H, Jiang C, et al. Research on the co-pyrolysis of coal gangue and coffee industry residue based on machine language: interaction, kinetics, and thermodynamics. *Sci Total Environ.* 2022;804:150217.
77. Mishra RK, Sahoo A, Mohanty K. Pyrolysis kinetics and synergistic effect in co-pyrolysis of *Samanea saman* seeds and polyethylene terephthalate using thermogravimetric analyser. *Bioresour Technol.* 2019;289:121608.
78. Balasundram V, Ibrahim N, Kasmani RM, et al. Thermogravimetric catalytic pyrolysis and kinetic studies of coconut copra and rice husk for possible maximum production of pyrolysis oil. *J Clean Prod.* 2017;167:218-228.
79. Toptas A, Yildirim Y, Duman G, Yanik J. Combustion behavior of different kinds of torrefied biomass and their blends with lignite. *Bioresour Technol.* 2015;177:328-336.
80. Kumar P, Subbarao PMV, Kala LD, Vijay VK. Thermogravimetry and associated characteristics of pearl millet cob and eucalyptus biomass using differential thermal gravimetric analysis for thermochemical gasification. *Therm Sci Eng Prog.* 2021;26:101104.
81. Tian H, Jiao H, Cai J, Wang J, Yang Y, Bridgwater AV. Co-pyrolysis of *Miscanthus sacchariflorus* and coals: a systematic study on the synergies in thermal decomposition, kinetics and vapour phase products. *Fuel.* 2020;262:116603.
82. Ming X, Xu F, Jiang Y, et al. Thermal degradation of food waste by TG-FTIR and Py-GC/MS: pyrolysis behaviors, products, kinetic and thermodynamic analysis. *J Clean Prod.* 2020;244:118713.
83. Xu Y, Chen B. Investigation of thermodynamic parameters in the pyrolysis conversion of biomass and manure to biochars using thermogravimetric analysis. *Bioresour Technol.* 2013;146:485-493.
84. Inayat A, Jamil F, Ahmed SF, et al. Thermal degradation characteristics, kinetic and thermodynamic analyses of date palm surface fibers at different heating rates. *Fuel.* 2023;335:127076.
85. Khan WUH, Khoja AH, Gohar H, et al. In depth thermokinetic investigation on co-pyrolysis of low-rank coal and algae consortium blends over CeO₂ loaded hydrotalcite (MgNiAl) catalyst. *J Environ Chem Eng.* 2022;10(5):108293.
86. Qiu S, Zhang S, Zhou X, et al. Thermal behavior and organic functional structure of poplar-fat coal blends during co-pyrolysis. *Renewable Energy.* 2019;136:308-316.
87. Liu Y, Song Y, Fu J, et al. Co-pyrolysis of sewage sludge and lignocellulosic biomass: synergistic effects on products characteristics and kinetics. *Energy Convers Manage.* 2022; 268:116061.

SUPPORTING INFORMATION

Additional supporting information can be found online in the Supporting Information section at the end of this article.

How to cite this article: Khoja AH, Gohar H, Khan WUH, et al. Exploring copyrolysis characteristics and thermokinetics of peach stone and bituminous coal blends. *Energy Sci Eng.* 2023;1-22. doi:10.1002/ese3.1583